Modeling the resolution of inexpensive, novel non-seismic geophysical monitoring tools to monitor CO_2 injection into Coal Beds

as a part of the report on

Stored CO_2 and Methane Leakage Risk Assessment and Monitoring Tool Development: CO_2 Capture Project Phase 2 (CCP2)

Type of Report:	Final Report
Reporting Period Start Date:	June 2005
Reporting Period End Date:	September 2008
Principal Author(s):	Erika Gasperikova, Research Scientist G. Michael Hoversten, Staff Scientist
Date Report was issued:	September 2008
Submitting Organization:	Lawrence Berkeley National Laboratory
Address:	One Cyclotron Road Mail Stop 90R1116 Berkeley, CA 94720

1. Abstract

A sensitivity study of gravity and electromagnetic (EM) techniques, and amplitude vs. angle (AVA) analysis for CO_2 movement in coal beds was based on the SECARB pilot test planned in the Black Warrior basin in Alabama. In the area of interest, coalbed methane is produced mainly from the Black Creek, Mary Lee, and Pratt coal zones at depths between 400 and 700 m and approximately 3 m thick on average. The permeability of coal in the Black Warrior basin decreases exponentially with depth as overburden stress increases. The permeability of the top layer is 100 mD, while the permeability of the deepest layer is around 1 mD. The pilot field test will include injecting a total of 1000 tons of CO_2 into these three coal zones (~300 tons to each zone). The density, sonic and resistivity well-logs from a deep disposal well a couple of miles from the pilot test site were used to create background (pre-injection) models. Our laboratory measurements of seismic velocity and electrical resistivity as a function of CO_2 saturation on coal core samples were used to provide a link between the coalbed CO_2 flow simulation models and the geophysical models. The sensitivity studies showed that while the response to the 300 tons of CO_2 injected into a single layer wouldn't produce measurable surface response for either gravity or EM, the response due to an industrial-size injection would produce measurable surface signal for both techniques. Gravity inversion results illustrated that, provided we can collect high-quality gravity data in the field and we have some a priori information about the depth of the reservoir, we can recover the spatial location of CO_2 plume correctly, although with the smoothing constraint of the inversion, the area was slightly overestimated, resulting in an underestimated value of density change. AVA analysis showed that by inverting seismic and EM data jointly, much better estimates of CO_2 saturation can be obtained, especially in the third injection zone, where seismic AVA data fail to detect the high CO_2 saturation. Analysis of spatial resolution and detectability limits show that gravity and EM measurements could, under certain circumstances, be used as a lower-cost alternative to seismic measurements.

2. Table of Contents

3. List of Figures and Tables

4. Introduction

Previous analysis of the spatial resolution and detectability limits of non-seismic geophysical techniques carried out as part of the "Novel geophysical monitoring" project of the first phase of the Carbon Capture Project (CCP-1) found that surface and borehole based electromagnetic (EM) and gravity measurements could, under certain circumstances, be used as a lower cost alternative to seismic geophysics (Gasperikova and Hoversten, 2006). An analysis of the cost of gravity and EM surveys needed for monitoring of enhanced oil recovery (EOR) projects showed them to be ten times less expensive than conventional 3D seismic surveys. The reduction in cost is accompanied by a reduction in spatial resolution and thus the applicability of non-seismic techniques is dependent on site specifics and the monitoring questions that need to be answered.

The work under CCP-1 was limited to a few generic models and a single case study of proposed CO_2 EOR/sequestration of the Schrader Bluff field on the North Slope of Alaska. In this project we evaluated gravity and EM techniques, and amplitude vs. angle (AVA) analysis for monitoring of CO_2 enhanced coal bed methane (CBM) production. The models were based on the Deerlick Creek Field pilot test design. In the area of interest, coalbed methane is produced mainly from the Black Creek, Mary Lee, and Pratt coal zones at depths between 400 and 700 m and approximately 3 m thick on average. The pilot field test will include injecting a total of 1000 tons of CO_2 into these three coal zones (~300 tons to each zone). Flow simulations were provided by Sproule Associates. LBNL laboratory measurements, carried out independently from this project, of seismic velocity and electrical resistivity as a function of CO_2 saturation on a coal core sample were used as a link between the coal bed CO_2 injection flow simulation results and the geophysical models.

We used the latest state-of-the-art forward and inverse capabilities for gravity, EM, and seismic data. We simulated gravity, EM, and seismic responses for the background (pre-injection) model, model with CO_2 injection into one coal zone, and model with CO_2 injection into three coal zones. We developed a new gravity inversion that uses a depth of the reservoir as *a priori* information, and solves for a smooth density variation inside the reservoir. The inversion of gravity data is very important, since construction of density contrast models significantly increases the amount of information that can be extracted from the gravity data. The simulated seismic data were imaged using industry-standard seismic processing techniques, and followed by acoustic AVA inversion for reservoir fluid properties. The CO_2 content predicted from the seismic data was compared to those obtained from a joint inversion of seismic and EM data.

5. Executive Summary

Significant potential exists for carbon sequestration and enhanced methane recovery in coalbed methane production scenarios. A sensitivity study of gravity and electromagnetic (EM) techniques, and amplitude vs. angle (AVA) analysis for CO_2 movement in coal beds was based on the SECARB pilot test planned in the Black Warrior basin in Alabama. Coal seams in the Black Warrior basin are distributed through a thick stratigraphic section and are clustered in a series of coal zones within the Lower Pennsylvanian Pottsville Formation. In the area of interest, coalbed methane is produced mainly from the Black Creek, Mary Lee, and Pratt coal zones at depths between 400 and 700 m and approximately 3 m thick on average. The permeability of coal in the Black Warrior basin decreases exponentially with depth as overburden stress increases. The permeability of the top layer is 100 mD, while the permeability of the deepest layer is around 1 mD. The pilot field test will include injecting a total of 1000 tons of CO_2 into these three coal zones (~300 tons to each zone).

A literature search for rock properties in an environment similar to the pilot test site revealed that no such information was available. Hence, we used our laboratory measurements of seismic velocity and electrical resistivity as a function of CO_2 saturation on coal core samples to link CO_2 flow simulation models to geophysical models for this study. Background (pre-injection) models were based on the density, sonic and resistivity well-logs from a deep disposal well a couple of miles from the pilot test site.

The sensitivity studies showed that while the response to the 300 tons of CO_2 injected into a single layer wouldn't produce measurable surface response for either gravity or EM technique, the response due to an industrial-size injection would produce measurable surface signal for both techniques.

Inversion of gravity data is very important, since construction of density contrast models significantly increases the amount of information that can be extracted from the gravity data. We developed a new gravity inversion and illustrated with the results that, provided we can collect high-quality gravity data in the field and we have some a priori information about the depth of the reservoir, we can recover the spatial location of CO_2 plume correctly, although with the smoothing constraint of the inversion, the area was slightly overestimated, resulting in an underestimated value of density change.

AVA analysis provides quantitative estimates of CO_2 saturation changes. Our results showed that by inverting seismic and EM data jointly, much better estimates of CO_2 saturation can be obtained, especially in the third injection zone, where seismic AVA data fail to detect the high CO_2 saturation.

Analysis of spatial resolution and detectability limits show that gravity and EM measurements could, under certain circumstances, be used as a lower-cost alternative to seismic measurements.

6. Experimental

The laboratory experiments (Kneafsey et al., 2005) were designed to gain a better understanding of brine displacement by carbon dioxide (CO_2) and to understand the flow behavior of CO_2 to allow evaluation and extension of numerical models. A horizontal coal core plug was used from the upper Cretaceous Ferron Sandstone member of the Macos Shale ("A" coal bed, Ivie Creek #11, Footage 293'4" to 294'0", Loc Sec 20, T 235 R6E Salt Lake Meridian). A series of measurements were made on the core while changing the core conditions.

Three tests were performed. The first test consisted of sorbing methane to the coal at the hydrostatic pressure at the depth the coal was retrieved, saturating the coal with brine (1g/l NaCl) at the same pressure. Following an equilibration time, the fluid pressure was reduced allowing gas to leave the core. In the second test, the same core was re-contacted with methane at a higher pressure, and introduced brine (1 g/l NaCl) saturated with CO_2 at 100 psi. Following this, pore pressure was reduced again. The third set of measurements was performed by introducing 1 g/l NaCl brine, and then CO_2 gas, CO_2 liquid, and 20% KI brine all at constant effective stress (confining pressure – pore pressure).

The test plug was a 39.1 mm diameter by 63.9 mm length coal plug from the above mentioned core with an air-dry mass of 99.50 g. The plug was cut perpendicular to the axis of the original drill core, thus it had a roughly horizontal orientation. Chips in the core were filled in with a sanded epoxy, and were impermeable and dense with respect to X-rays.

Several sets of measurements were made. Compressional and shear wave travel times were measured using Panametric D7253 transducers contained within one end cap in contact with the sample and detected by a duplicate transducer contained within the opposing end cap. Pulses were applied to the transmitting transducer with a pulse width of 1.8 microseconds and a voltage of 500 V using an Instrument Research Company Model M1k-20 1000V Pulser, and detected pulses were amplified by a Stanford Research Systems Model SR560 Low Noise Preamplifier and indicated on a Tektronix Digital Oscilloscope (TDS3012, 100 Mhz, 1.25GS/s).

Resistivity was measured using up to four ring electrodes in contact with the sample using a GenRad 1692 RLC meter and QuadTech 7400B Precision RLC Meter. The system was calibrated using water of known conductivity.

Permeability was deduced using flow rates indicated by Isco syringe pumps, core geometry, and Druck and Validyne pressure transducers.

X-ray CT scanning was performed on a modified Seimens Somaton High-Q third generation medical CT scanner with energy of 130KeV. Most scans were performed in the "inner ear mode" with a resolution of 0.3 x 0.3 x 1 mm (1 mm beam width). Scanning was performed on alternate 1 mm slices along the axis of the core.

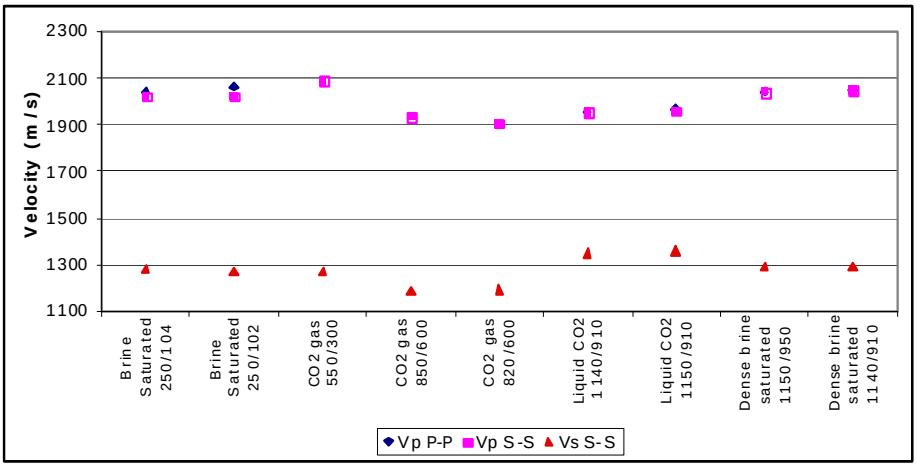

Figure 1. Compressional and shear wave velocities for the laboratory test conditions

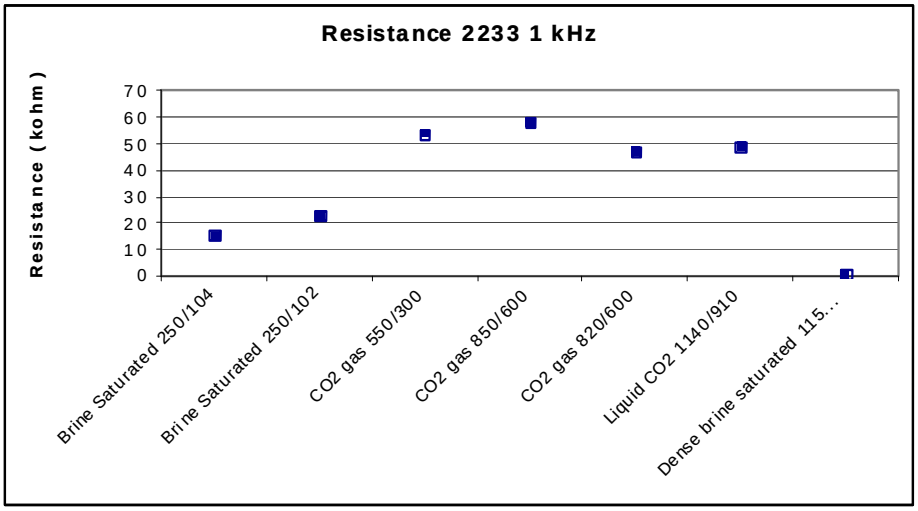

Figure 2. Resistances measured across electrodes 2 and 3 (2-wire method) for Test 3

The overall conclusions of the experimental data show that acoustic (Vp) and shear (Vs) velocities were reduced on the order of 10% by the CO_2 flood (Figure 1). Electrical resistivity increased by 160% in the core when flooded by CO_2 (Figure 2).

These experimentally determined values were used as end members of a linear trend for velocity and resistivity over the range from 0 to 100% CO_2 saturation. These experimentally determined functions were used to convert the flow simulations provided by Sproule Associates to the geophysical models used to determine the detectability and resolution for monitoring of the CO_2 flood.

7. Results and Discussion

Significant potential exists for carbon sequestration and enhanced methane recovery in coalbed methane production scenarios. Our study was motivated by a pilot test planned in the Black Warrior basin in Alabama. Coal seams in the Black Warrior basin are distributed through a thick stratigraphic section and are clustered in a series of coal zones within the Lower Pennsylvanian Pottsville Formation. Assessment of the CO_2 sequestration and enhanced recovery potential of coalbed methane in this area indicated that more than 5.9 Tcf of CO_2 could be sequestered, while increasing coalbed methane reserves by more than 20% (Pashin and Clark, 2006). In the area of interest, coalbed methane is produced mainly from the Black Creek, Mary Lee, and Pratt coal zones at depths between 400 and 700 m and approximately 3 m thick on average. The permeability of coal in the Black Warrior basin decreases exponentially with depth as overburden stress increases. The permeability of the top layer is 100 mD, while the permeability of the deepest layer is around 1 mD. The pilot field test will include injecting a total of 1000 tons of CO_2 into these three coal zones (~300 tons to each zone).

A literature search for rock properties in an environment similar to the pilot test site revealed that no such information was available. Hence, we used the density, sonic and resistivity well-logs from a deep disposal well that was drilled only a couple of miles from the pilot test site (Jack Pashin, Geological Survey of Alabama), and our laboratory measurement results to build models for this study.

(A) Gravity monitoring

The reduction in the vertical component of gravity is caused by increased CO_2 saturations reducing the bulk density of the coal layer. The spatial pattern of the change in the vertical component of gravity is directly correlated with the net change in density of the coal bed.

A simplified model was created to investigate if a variation in CO_2 saturation in a coal layer would produce a measurable surface gravity response. The model consisted of a 5 m thick coal layer with a density of 1435 kg/m^3 at a depth of 450 m. A plan view of the model is shown in Figure 3a, while the section view is shown in Figure 3b. The undisturbed coal layer is on the left, while a coal layer containing CO_2 is on the right.

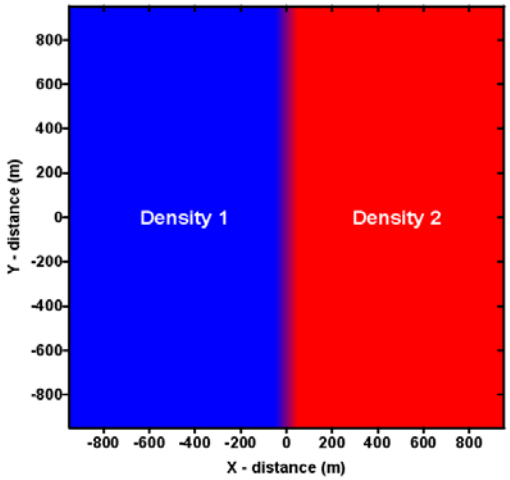

Figure 3a. Plan view of a density model with a coal layer with no CO_2 on the left and with CO_2 on the right

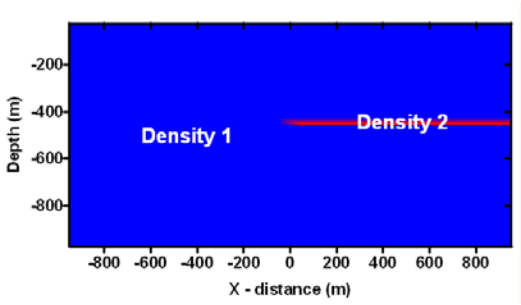

Figure 3b. Cross-section of a density model with a coal layer with no CO_2 on the left and with CO_2 on the right

Using values from the flow simulation model, we calculated the density of CO_2 at a temperature of 35°C (= 308 K = 95 F) and a pressure of 600 kPa using the NIST14 code (NIST, 1992). Under these conditions the density of CO_2 is 10.6 kg/ m^3. If we define CO_2 saturation as S_{CO2}, then the layer bulk density is:

$$\text{Density} = (1- S_{CO2})*\text{Density(coal)} + S_{CO2}*\text{Density}(CO_2)$$

We calculated values for 0, 10, 20, 50, 70, 80, and 90% of CO_2 saturation and the resulting densities are given in Table 1. The presence of CO_2 reduces the coal density, causing the decrease in the gravity response. Adsorption of CO_2 into coal can affect the matrix density, and hence the total density change could be smaller than we predicted.

Table 1. Coal layer density as a function of CO_2 saturation at temperature of 35°C and pressure of 600 kPa.

% CO_2	Density (kg/m^3)
0	1435.0
10	1291.6
50	721.8
70	437.9
80	295.5
90	153.0

The vertical component of the gravity response is defined as a difference between the model with and without CO_2 present. Figure 4 shows the surface gravity response (in μGal) for 10% of CO_2 saturation. The maximum gravity response is -14 μGal. The contact between area with and without CO_2 is clearly visible, and the surface gravity response can be measured using current technologies. A 5-10 μGal and 3.5 μGal survey accuracy have been reported for gravity surveys at Prudhoe Bay, Alaska (Hare et al., 1999; Brown et al., 2003). A repeatability of 2.5 μGal and detection threshold of 5 μGal for time-lapse variations was observed in gravity monitoring surveys of the Sleipner CO_2 sequestration site in the North Sea (Nooner et al., 2003).

Figures 5 and 6 are surface gravity responses for the model with 50% and 90 % of CO_2 saturation, respectively. For the model with 50% CO_2 saturation the maximum gravity response is -70 μGal while for the model with 90% CO_2 saturation the maximum gravity response is -125 μGal. Again, we can clearly distinguish areas with CO_2 present in both cases. Figures 4-6 illustrate that the surface gravity response decreases with increased CO_2 saturation. The presence of CO_2 reduces the layer density and that causes the decrease in the gravity response.

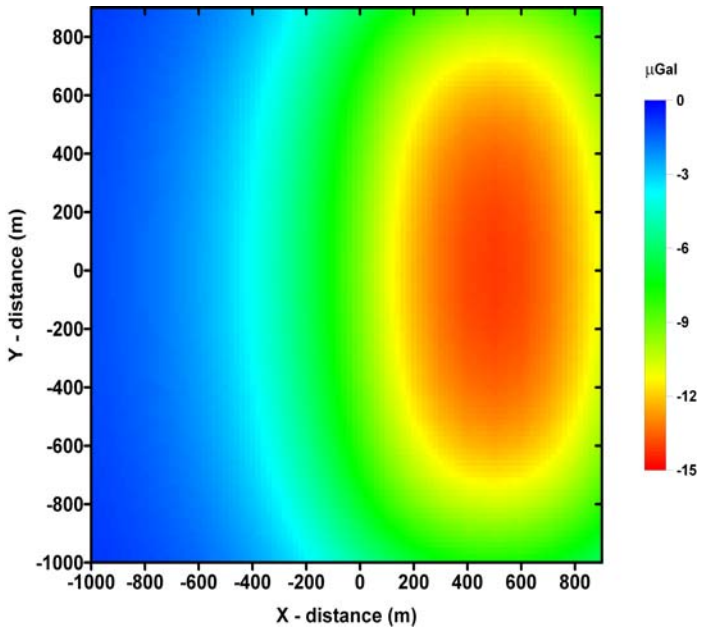

Figure 4. Surface gravity response (in μGal) for the coal layer in Figure 3 with 10% CO_2 saturation

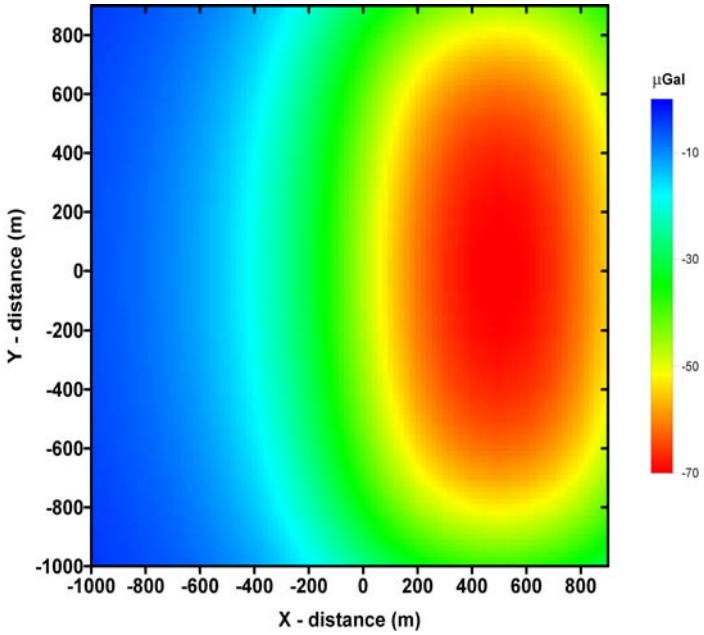

Figure 5. Surface gravity response (in μGal) for the coal layer in Figure 3 with 50% CO_2 saturation

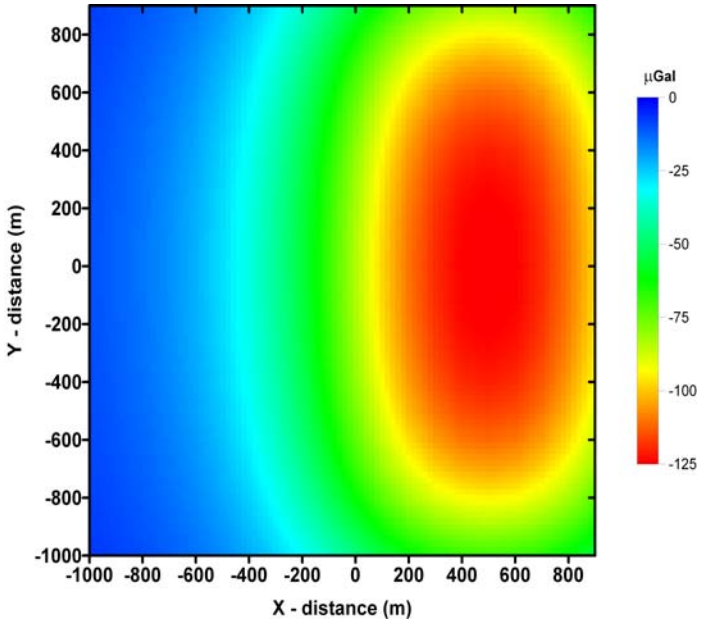

Figure 6. Surface gravity response (in μGal) for the coal layer in Figure 3 with 90% CO_2 saturation

In the proposed pilot test the amount of injected CO_2 is limited, and Sproule Associates ran flow simulation models for CO_2 injection into three coal layers. CO_2 mole fractions in the three coal layers at the end of simulation are shown in Figures 7-9. Figure 7 is a plan view of CO_2 mole fractions for the coal layer at the depth of ~400 m, Figure 8 for the layer at ~ 600 m, and Figure 9 for the layer at ~750 m.

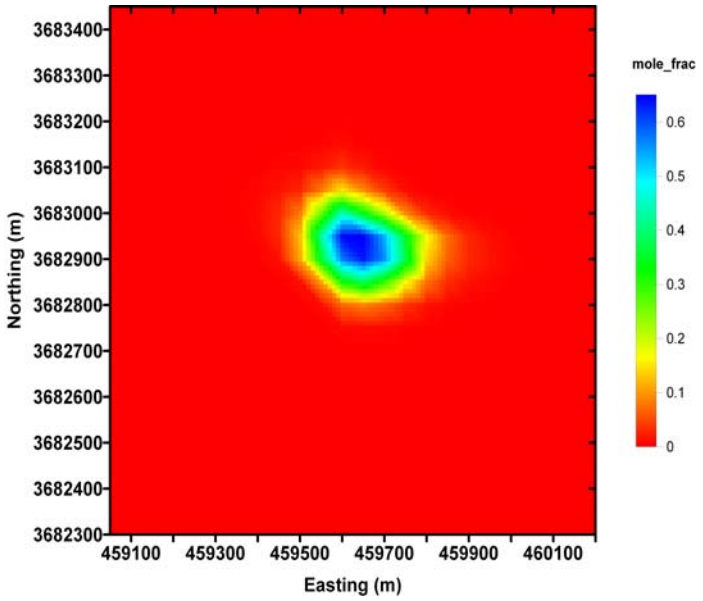

Figure 7. Plan view of CO_2 mole fractions for the coal layer at a depth of ~ 400 m at the end of simulation (from Sproule Associates)

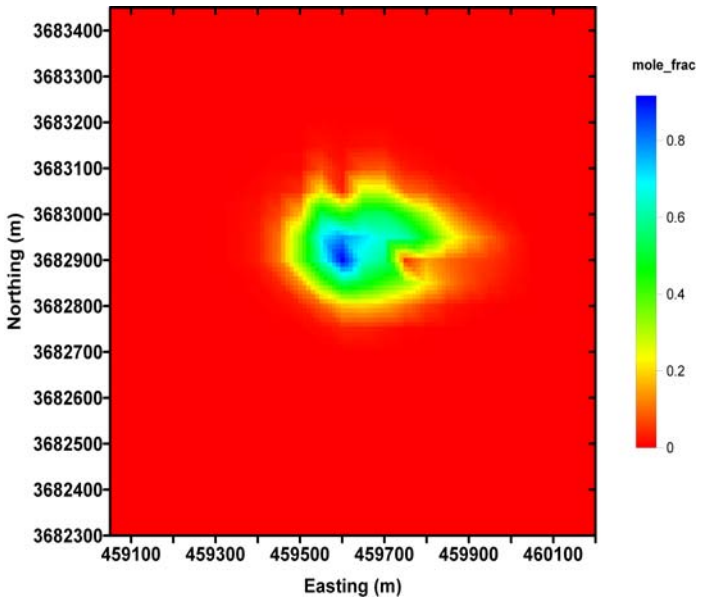

Figure 8. Plan view of CO_2 mole fractions for the coal layer at a depth of ~ 600 m at the end of simulation (from Sproule Associates)

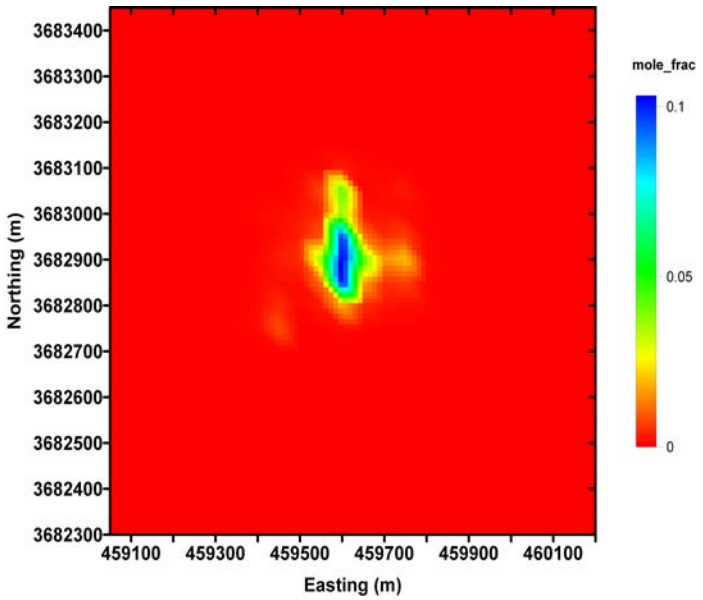

Figure 9. Plan view of CO_2 mole fractions for the coal layer at a depth of ~ 750 m at the end of simulation (from Sproule Associates)

Flow simulation models (Figure 7-9) showed that the highest CO_2 mole fractions and the largest spatial extent of CO_2 exist in the upper two coal layers. CO_2 in the deepest layer hardly moved from the injection well, presumably due to very low permeability. Based on these simulations, our reference density model was a coal layer with 95% water saturation and 5% residual gas saturation. We assumed that water in fractures is replaced by CO_2 and neglected any changes in the matrix density. We calculated the surface gravity response for each of the three layers independently, and then for all of them together. Figure 10a shows a plan view, and Figure 10b shows a section view of the model. The coal layer at the depth of ~ 400 m, 600 m, and 750 m, respectively, is 3 m thick, and CO_2 anomaly is 300 × 200 m wide, and has 50% CO_2 saturation.

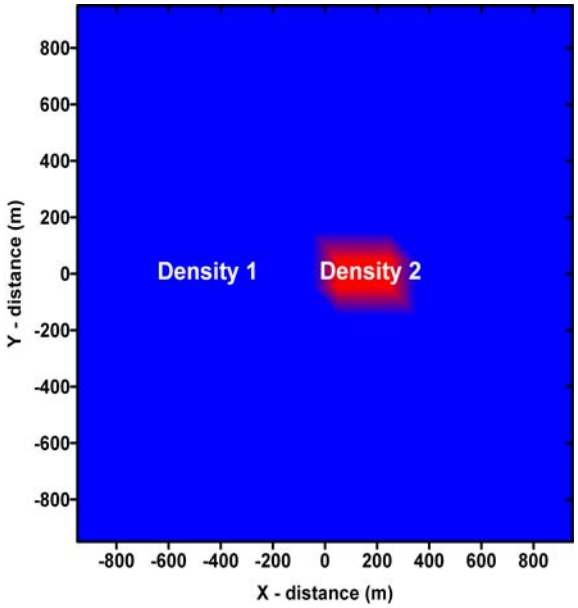

Figure 10a. Plan view of a density model based on a flow simulation model

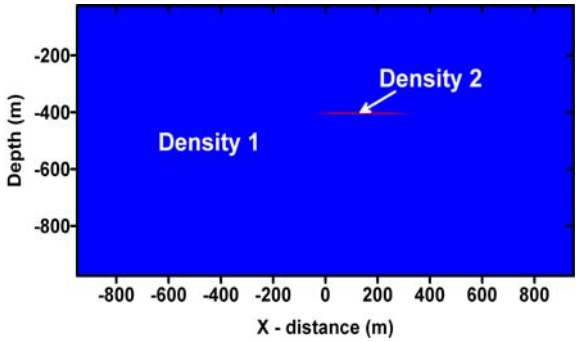

Figure 10b. Cross-section of a density model based on a flow simulation model

Figure 11 shows the surface gravity response for the CO_2 plume at the depth of 400 m. The maximum response is -5 μGal, which is on the edge of detectability in the field. Gravity anomalies decay with the inverse square of the distance from their source, hence the same plume at 600 m or 750 m produces even smaller surface gravity response (not shown) and hence it would be difficult to detect in the field.

However, if the layer thickness at the depth of 400 m would be 6 m instead of 3 m and the CO_2 plume had the same lateral extent (300×200 m) the maximum surface gravity response would be -10 μGal. This anomaly response is above the detection threshold and therefore it would be measurable in the field. The surface gravity response from a 6 m thick layer is shown in Figure 12. Similarly, surface gravity measurements would be above the detection threshold when all three layers are present. In this case, the thickness of each layer is 3 m, the lateral extent is 300×200 m, each layer contains 50% of CO_2, and they are at the depth of 400, 600, and 750 m, respectively. The surface gravity response of this model is shown in Figure 13. As mentioned earlier, the surface gravity response decreases with the square of the distance to the source. Hence, although the model contains identical CO_2 anomalies in three different layers, most of the response comes from the layer at 400 m, then from the layer at 600 m, and the least from the layer at 750 m.

The deepest coal layer, at the depth of 750 m, with the same lateral extent and properties as described above, would be detectable by surface gravity only if its thickness was 18 m. The surface gravity response for this case is shown in Figure 14.

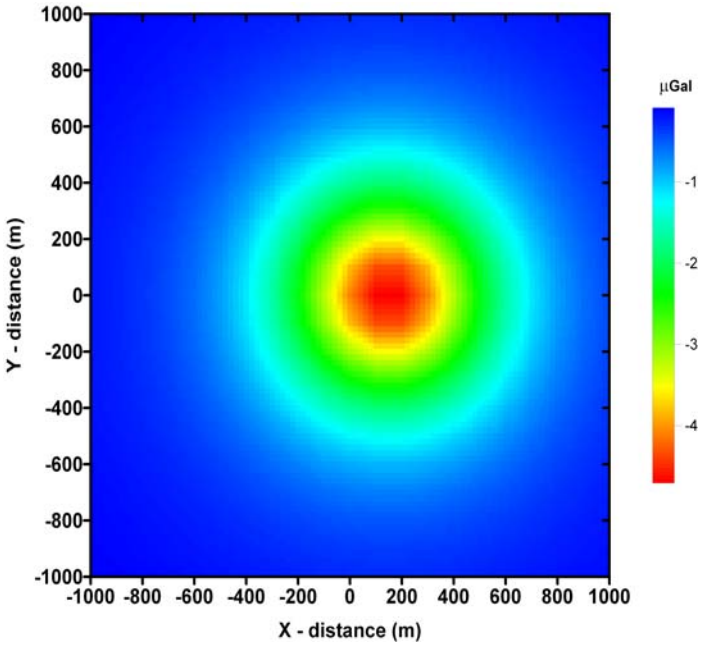

Figure 11. Surface gravity response (in μGal) for the model in Figure 10. The coal layer at the depth of 400 m is 3 m thick, CO_2 plume is 300×200 m wide, and it contains 50% of CO_2.

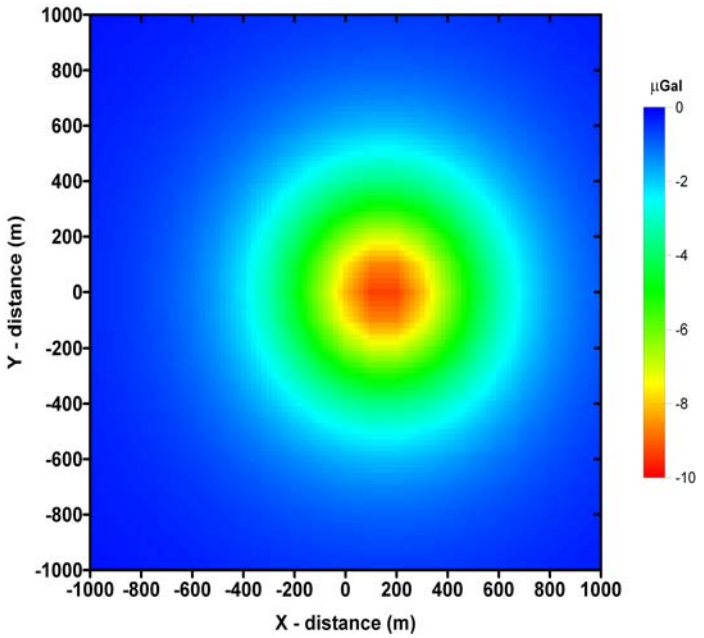

Figure 12. Surface gravity response (in μGal) for the model in Figure 10. The coal layer at the depth of 400 m is 6 m thick, CO_2 plume is 300×200 m wide, and it contains 50% of CO_2.

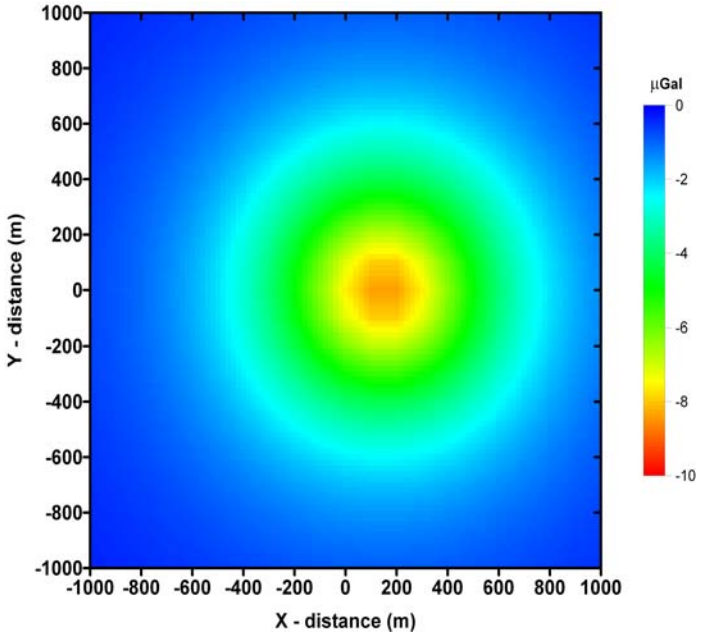

Figure 13. Surface gravity response (in µGal) for the model with three coal layers at depths of 400 m, 600 m, and 750 m. Each layer is 3 m thick, CO_2 plume is 300×200 m wide, and it contains 50% of CO_2.

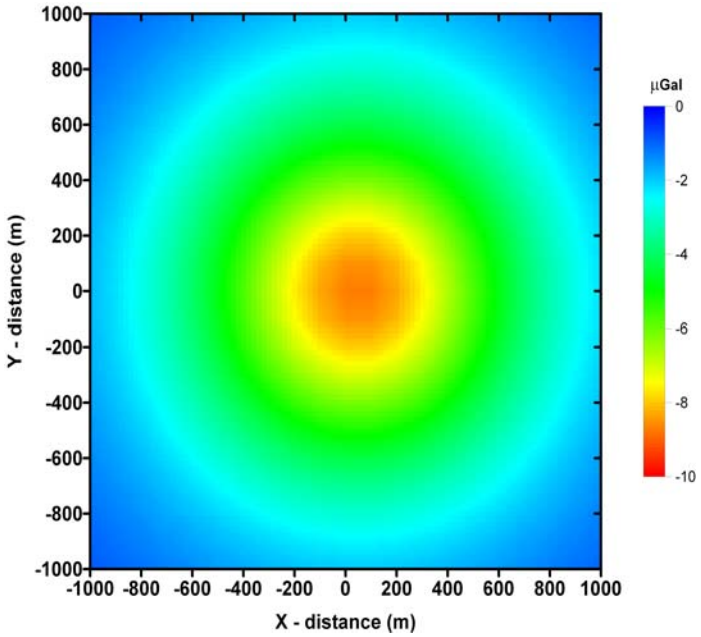

Figure 14. Surface gravity response (in µGal) for the coal layer at the depth of 750 m. The layer is 18 m thick, CO_2 plume is 300×200 m wide, and it contains 50% of CO_2.

Gravity inversion

Inversion of gravity data is very important, since construction of density contrast models significantly increases the amount of information that can be extracted from the gravity data. However, one substantial difficulty with the inversion of gravity data is its inherent non-uniqueness and lack of inherent depth

resolution. This difficulty can be overcome by introduction of *a priori* information. We adopted the approach described by Smith et al. (1999) for magnetotelluric data inversion, in which the top and base of the reservoir are known, and we invert for a smooth density variation inside the reservoir. The inversion result is a cumulative density change in the reservoir as a function of x and y coordinates.

To illustrate the whole approach we took the CO_2 mole fractions model shown in Figure 15, and created a density model shown in Figure 16. We calculated the surface gravity response to this model (Figure 17), and then ran the inversion.

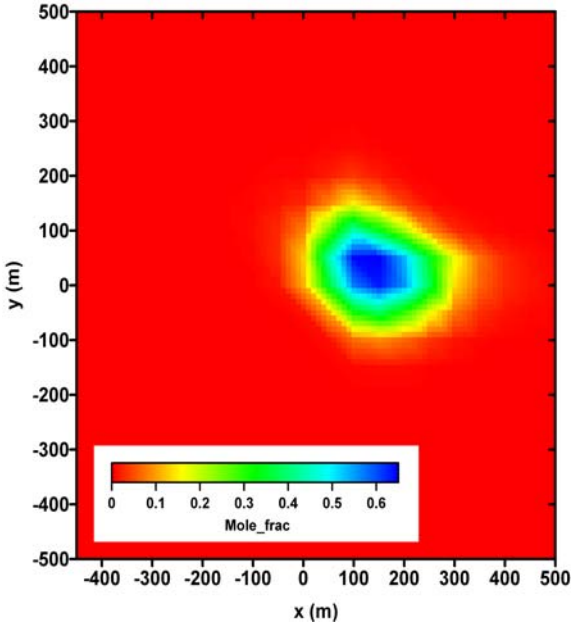

Figure 15: Plan view of CO_2 mole fractions in the coal layer at a depth of 400 m (from Sproule Associates)

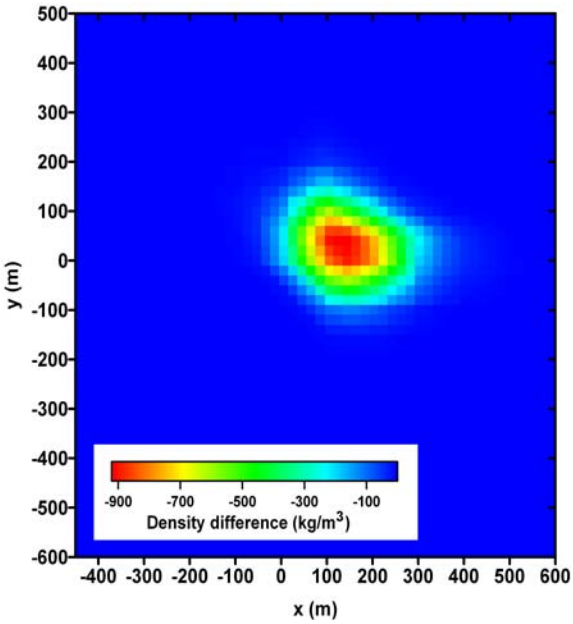

Figure 16: Plan view of a density model (kg/m^3) based on the flow simulation model in Figure 15

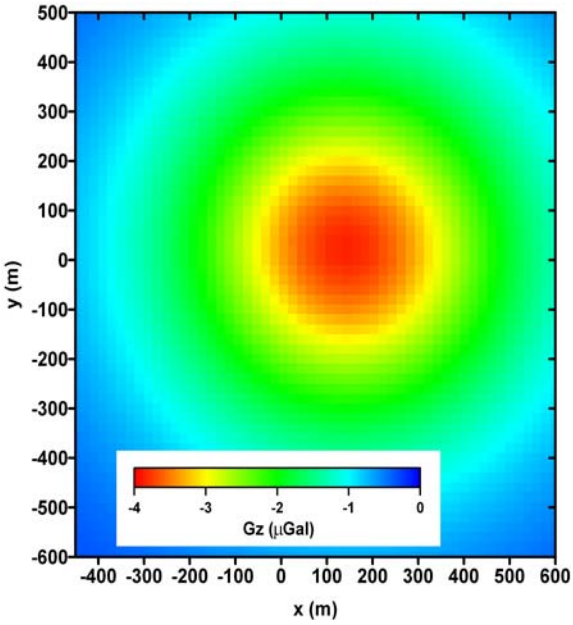

Figure 17: Surface gravity response (μGal) of the model in Figure 16

Figure 18 shows inversion results from surface gravity data shown in Figure 17. The location of the CO_2 plume was recovered correctly, although with the smoothing constraint of the inversion, the area was slightly overestimated, resulting in an underestimated value of density change (Figure 18a). The inversion of gravity data from Figure 17 with 1 μGal random noise (25% of peak value) added results in the correct location of the CO_2 plume; however the density contrast cannot be resolved (Figure 18b). The true density difference is shown by white contours.

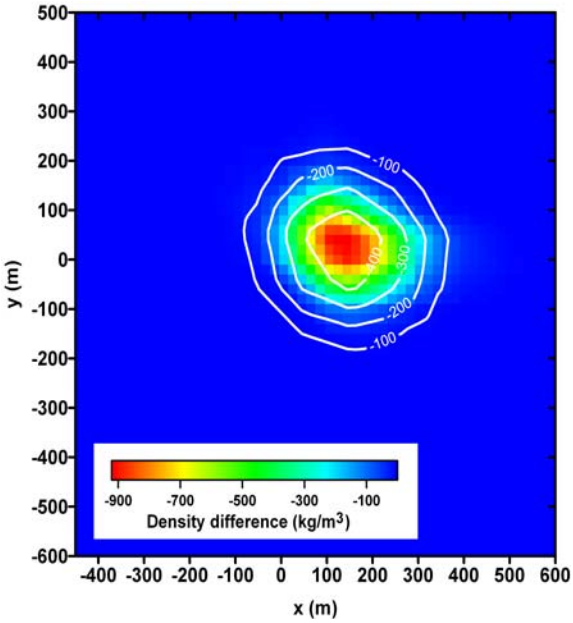

Figure 18a. Density change (kg/m^3) as a function of x and y coordinates recovered by inversion of the data shown in Figure 17

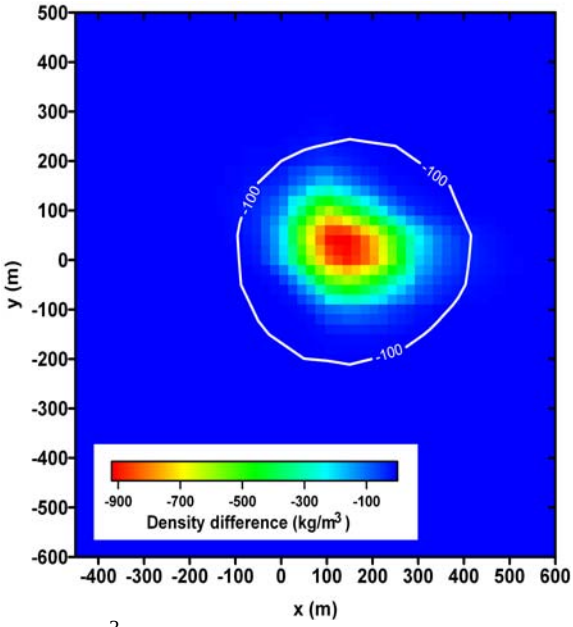

Figure 18b. Density change (kg/m^3) as a function of x and y coordinates recovered by inversion of the gravity data in Figure 17 with 1 μGal random noise (25% of peak response) added

(B) EM monitoring

The electrical resistivity of reservoir rocks is highly sensitive to changes in water and gas saturation. This high sensitivity can be exploited by EM techniques, in which the response is a function of the earth's electrical resistivity. One technique uses a grounded electric dipole energized with an alternating current at a given frequency (i.e. 1 Hz) to produce time-varying electric and magnetic fields that can be measured on the earth's surface. In this configuration the electric dipole consists of two steel electrodes (1 m^2 plates or sections of drill pipe) buried at a shallow depth (1–10 m) separated by 100 m and connected by cable to a low-power generator (a portable 5,000 W generator is sufficient). A setup schematic is shown in Figure 19a, and instruments' photos are shown in Figure 19b. The measured data consist of the electric field at a given separation from the transmitter, acquired on the surface or within the near surface.

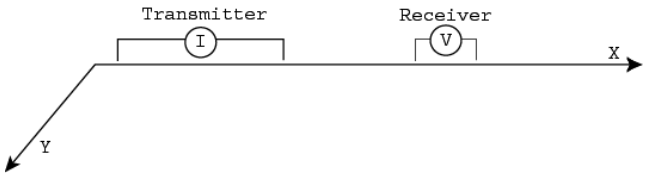

(a)

(b)

Figure 19. EM survey (a) schematic, (b) equipment photos.

As described earlier, the pilot study area contains three main coal layers – Pratt, Mary Lee, and Black Creek. According to the annotated coal lithology log of J.D. Jobson 24-14 #11 Well, that's a part of the SECARB II project design package, the top of the Pratt zone is at the depth of 396 m and the injection zone is between 405 and 442 m, the top of the Mary Lee zone is at 574 m and the injection zone is between 592 and 610 m, and the top of the Black Creek zone is at 673 m, and the injection zone is between 750 and 760 m. We used the resistivity log from a deep disposal well that was drilled a couple of miles from the pilot test site, to build our background resistivity model. We used results of our previous laboratory measurements to estimate how the presence of CO_2 influences coalbed resistivities. Our laboratory results show that CO_2 can cause up to 150% resistivity increase in coal. Assuming that the layers within each injection zone will be influenced by the presence of CO_2 in a manner similar to that in the laboratory measurements, we created our CO_2 model. Resistivity values as a function of depth for both the background and CO_2 models are given in Table 2, and plotted in Figure 20. The blue color in Figure 20 represents the background model, while the red color represents the CO_2 model.

Table 2. Resistivity values as a function of depth for the background and CO_2 models

Depth (m)	Resistivity (Ohm-m) background model	Resistivity (Ohm-m) CO_2 model
0	60	60
396	100	250
402	2000	5000
405	100	250
408	1000	2500
411	100	250
427	400	1000
430	70	70
451	300	300
457	2000	2000
460	300	300
482	1500	1500
509	70	70
530	300	300
536	90	90
552	30	30

555	100	100
561	30	30
564	75	190
637	40	40
658	600	600
661	60	60
744	150	400
762	60	60

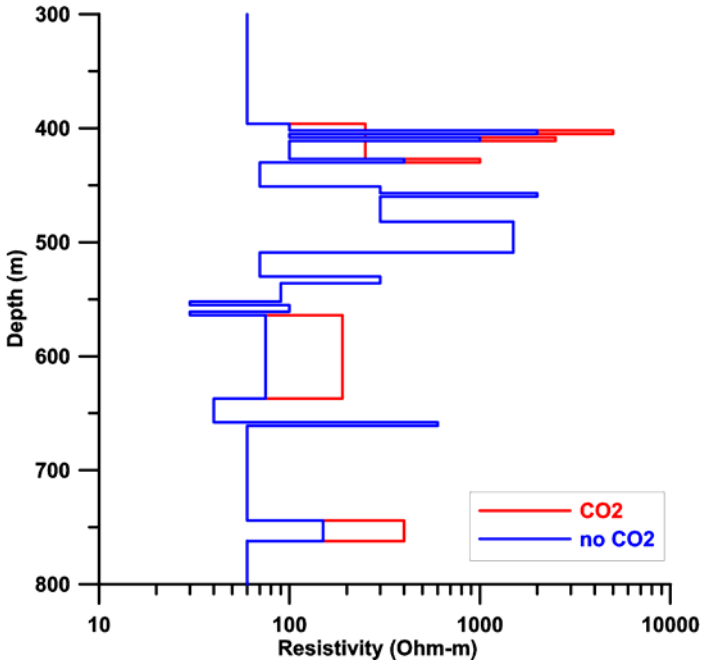

Figure 20. Resistivity profiles as a function of depth for the background model in blue, and CO_2 model in red.

We calculated responses of both models using an electric point dipole as a source (transmitter) and an electric point dipole as a receiver. Both "in-line" and "broad-side" responses were calculated for transmitter - receiver offsets up to 4 km. The transmitter was oriented in the x-direction. When both the transmitter and receiver are on the same line (i.e. y(Tx)=0 and y(Rx)=0), the configuration is called "in-line" configuration. When the transmitter is on a different line than the receiver (i.e. y(Tx)=0 and y(Rx)=150), the configuration is called "broad-side" configuration. The in-line responses were much smaller than the broad-side responses; therefore we present here only the broad-side responses. The broad-side Ex and Ey data for models with and without CO_2 are presented in Figures 21 and 22, respectively.

In both figures, the red dashed line is a magnitude of the real component of the electric field for the model with CO_2 while the blue solid line is for the model without CO_2. The purple dashed line is a magnitude of the imaginary component of the electric field for the model with CO_2 while the green solid line is for the model with no CO_2. The results show the maximum response for offsets larger than 2 km. The change due to CO_2 presence in the real component of Ex is 10-20%, and 5-10% in the imaginary component of Ex. In the case of Ey, the real component is 10-20% larger, and the imaginary component is 100-200% larger for the model with CO_2.

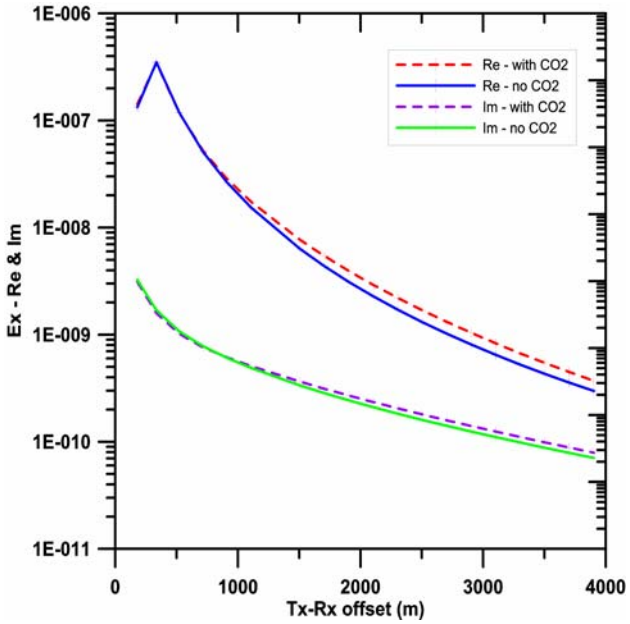

Figure 21. Real and imaginary component of Ex field for models in Table 2

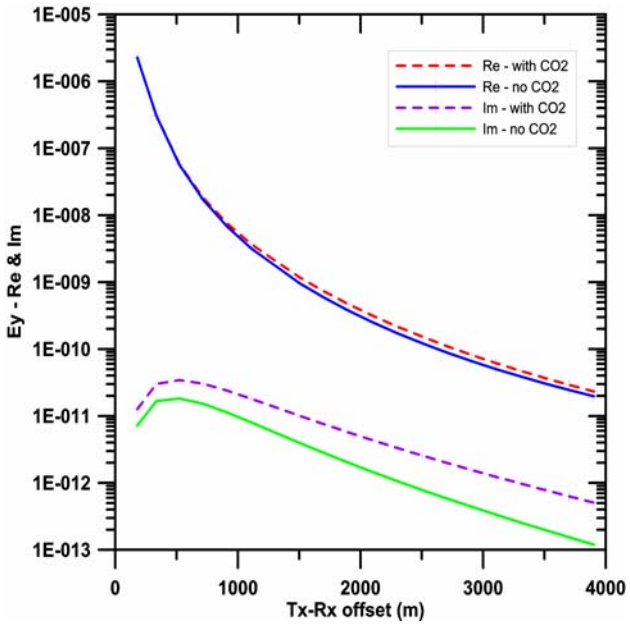

Figure 22. Real and imaginary component of Ey field for models in Table 2

The amplitude and phase plots for the broad-side Ex-component are shown in Figures 23a and 23b, while the amplitude and phase plots for the broad-side Ey-component are shown in Figures 24a and 24b. Responses to individual injections zones (not shown) were smaller than the response to all three zones together.

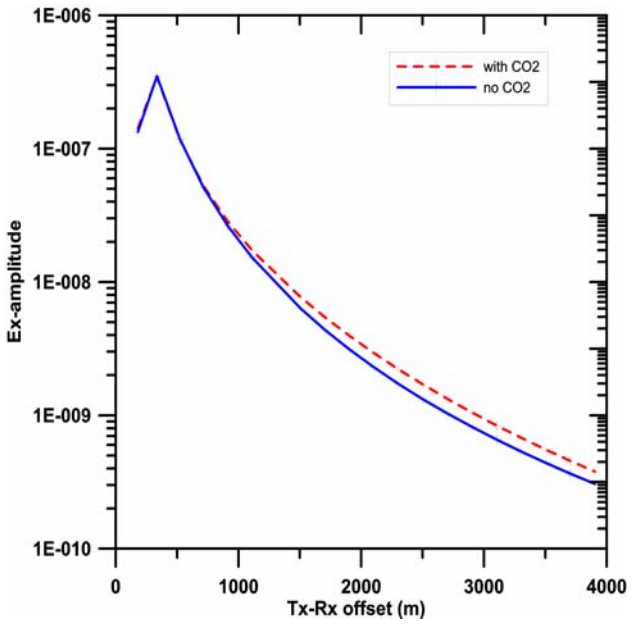

Figure 23a. Amplitude of Ex field for models in Table 2

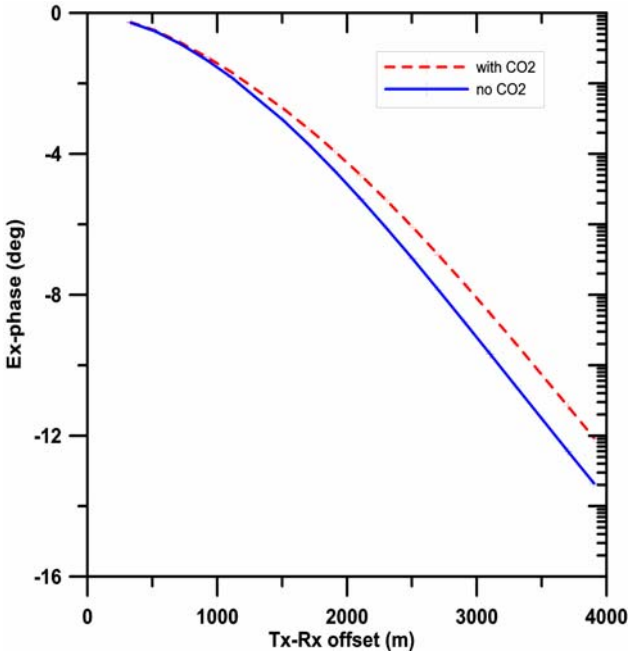

Figure 23b. Phase of Ex field for models in Table 2

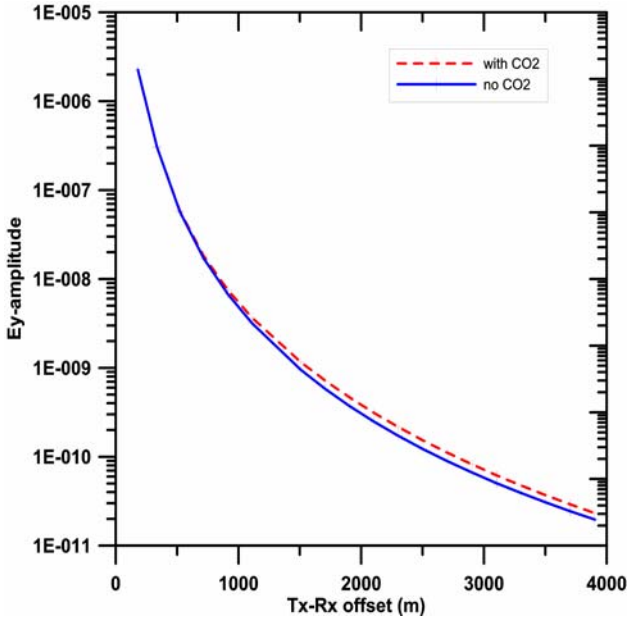

Figure 24a. Amplitude of Ey field for models in Table 2

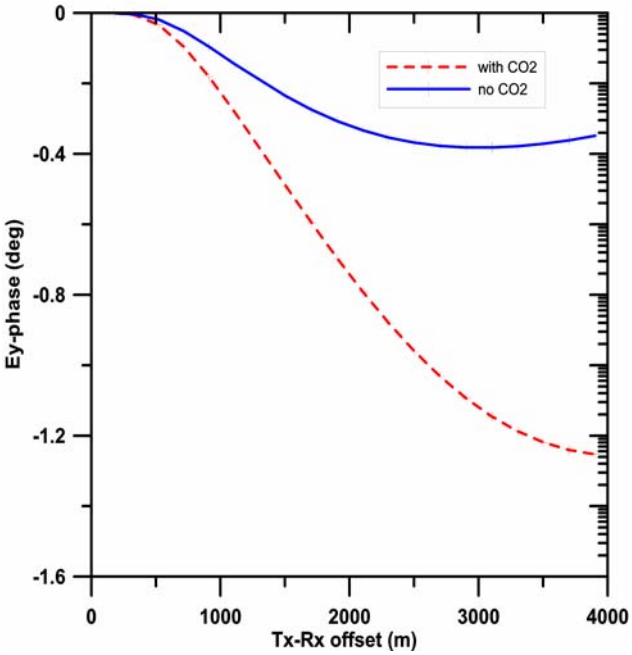

Figure 24b. Phase of Ey field for models in Table 2

(C) Amplitude vs. Angle (AVA) Analysis

It has been recognized that monitoring of field-scale CO_2 saturation is important for CO_2 sequestration. Time-lapse geophysical methods, for example, surface seismic and EM, have the potential of providing this information, and hence being candidate monitoring tools. In this section, we investigate the feasibility of using time-lapse seismic AVA and EM data to monitor CO_2 injection into coal beds through synthetic case studies. We assume that the background information, such as thickness of each layer, seismic P- and

S-wave velocities, density, and electrical resistivity can be obtained from borehole logging. The background models for seismic attributes and electrical properties may be different, but the CO_2 injection zones are located at roughly the same depths in both models.

Seismic data

Synthetic seismic data were generated using a 2D finite-difference staggered-grid code which models elastic wave propagation in arbitrarily inhomogeneous media with a 18 Hz Gaussian derivative source wavelet (Levander, 1988) for the following three cases: (1) background (pre-injection) model (Model-0) using the well logs from a nearby well, (2) model with a 10% decrease in P-wave velocity and a 5% decrease in density in the top injection zone (Model-1), and (3) model with a 10% decrease in P-wave velocity and a 5% decrease in density in all the three injection zones (Model-2). The decrease in P-wave velocity and density due to the presence of CO_2 was based on our laboratory measurements on coal samples (Kneafsey et al., 2005). Figure 25a shows the seismic P-wave velocity cross-section when CO_2 is injected into the top injection zone, while Figure 25b shows the seismic P-wave velocity cross-section when CO_2 is injected into all three injection zones. The CO_2 plume was 300 m wide from x = 850 m to x= 1150 m.

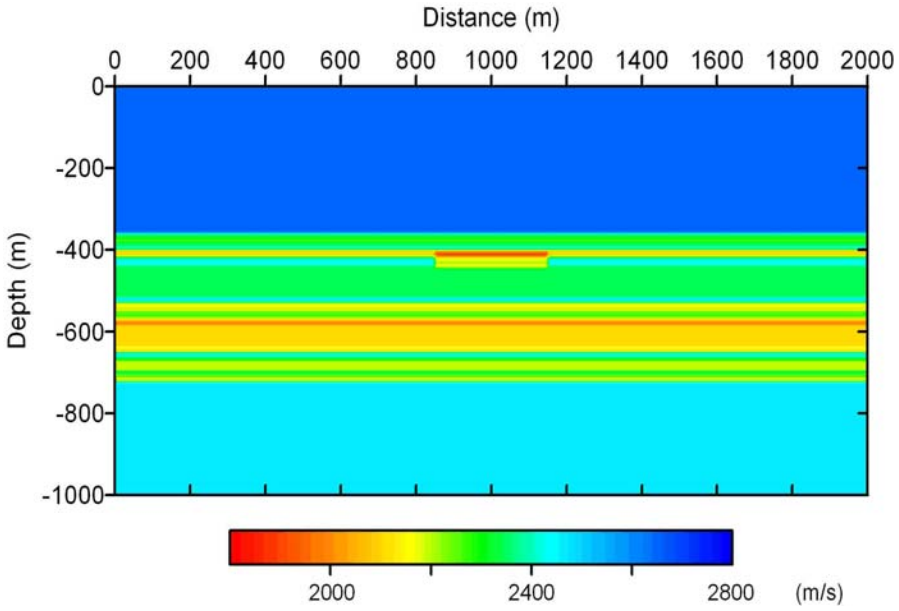

Figure 25a. 2D seismic P-wave velocity model for CO_2 injection in the top injection zone

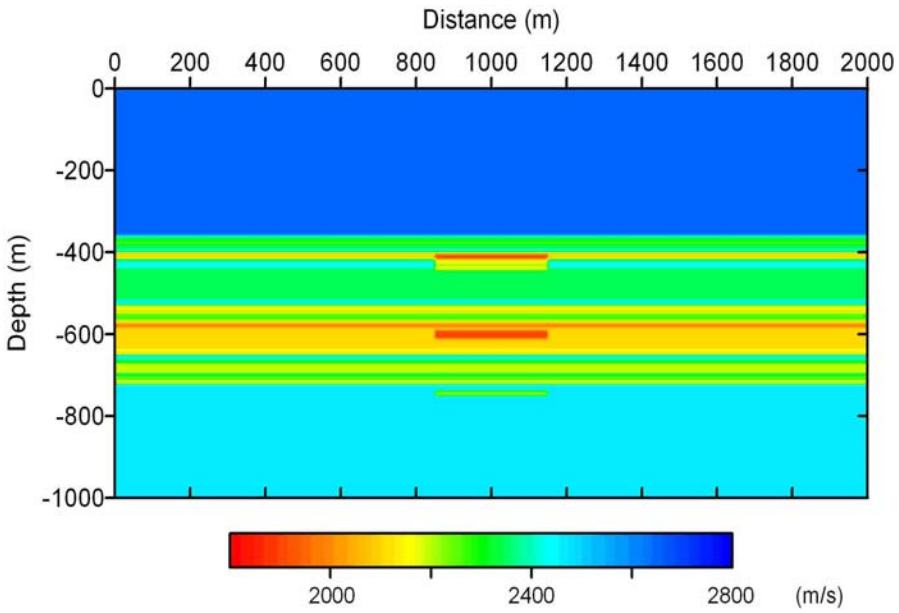

Figure 25b. 2D seismic P-wave velocity model for CO_2 injection into all three injection zones

After normal moveout (NMO) correction, we created a common depth point (CDP) stack, and from that AVA data. We first generated seismic AVA for the background model, and then we assumed that the injection zone(s) had 95% CO_2 saturation, and generated seismic AVA responses again. The normalized differences in seismic AVA responses between the model with CO_2 plume and the background model were our time-lapse AVA data. Detail description of the approach is given in Appendix 1. As only the first four incident angles (corresponding to 0, 1.9, 3.8, and 5.7 degrees, respectively) had responses to all the zones, we only used them for inversion. At this point, the AVA inversion is using 1D numerical codes, hence we calculated 1D seismic data as well and compared them to 2D data.

The 1D seismic data were calculated by convolving seismic reflectivity with the Gaussian derivative wavelet with the center frequency of 18 Hz. Seismic AVA reflectivity is an explicit function of seismic P- and S-wave velocities and density in the given layers. We used the Zoeppritz's equations (Aki and Richards, 1980) to model the reflectivity, which is a function of seismic P- and S-wave velocities and density.

A comparison of normalized differences in seismic AVA data for the model with a CO_2 plume in the top injection zone calculated using 1D and 2D numerical methods is shown in Figure 26a, while the same comparison for the model with CO_2 present in all three injection zones is shown in Figure 26b. Figure 26 shows that 1D convolution model provides a good approximation to 2D data at small angles.

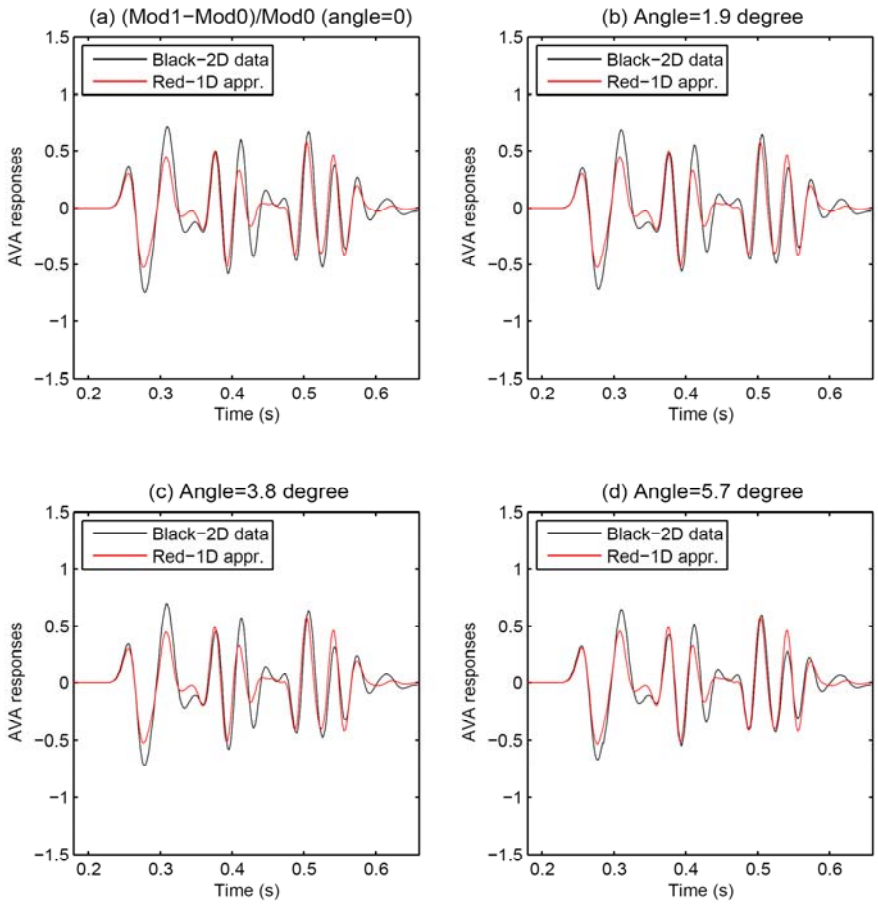

Figure 26a. Comparison of differences in normalized seismic AVA data, (Model-1 - Model-0)/Model-0 for four angles, where the black curves are calculated using the 2D numerical methods and the red curves are calculated using the 1D convolution method

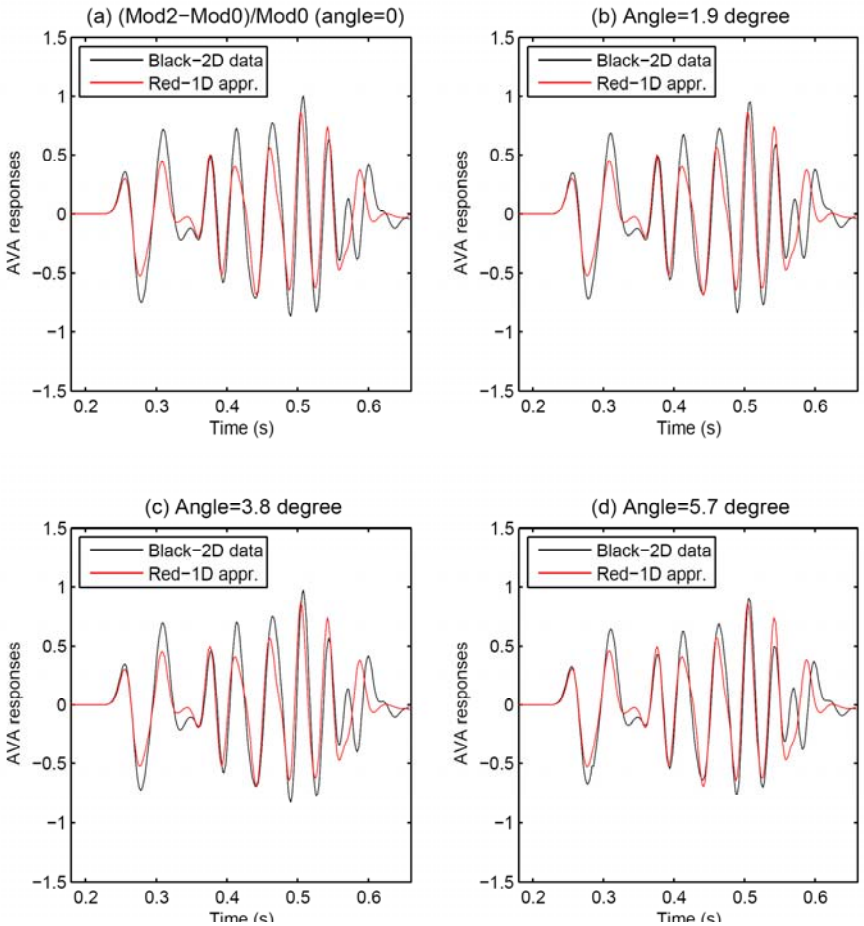

Figure 26b. Comparison of differences in normalized seismic AVA data, (Model-2 - Model-0)/Model-0 for four angles, where the black curves are calculated using the 2D numerical methods and the red curves are calculated using the 1D convolution method

EM data

Synthetic EM data were generated using 2D numerical methods (Newman and Alumbaugh, 1997) at two frequencies (1 Hz and 10 Hz), with five transmitter locations (-2000 m, -1900 m, -1800 m, -1700 m, and -1600 m), and 60 receivers located from -1000 m to 1900 m with a separation of 50 m. Again, three cases were considered: (1) background (pre-injection) model (Mod0) using the well logs from the nearby well, (2) model with a 150% increase in resistivity in the top injection zone (Mod1), and (3) model with a 150% increase in resistivity in all the three injection zones (Mod2). The increase in resistivity due to the presence of CO_2 was based on our laboratory measurements on coal samples (Kneafsey et al., 2005). Figure 27a shows the resistivity cross-section when CO_2 was injected into the top injection zone, while Figure 27b shows the resistivity cross-section when CO_2 was injected into all three injection zones. The CO_2 plume was 300 m wide from x = 850 m to x= 1150 m.

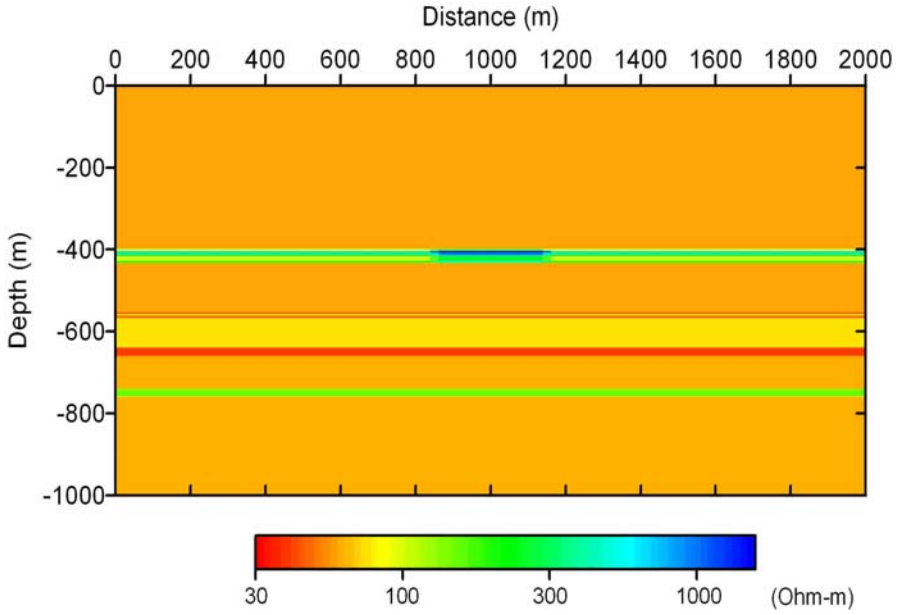

Figure 27a. 2D resistivity model for CO_2 injection in the top injection zone

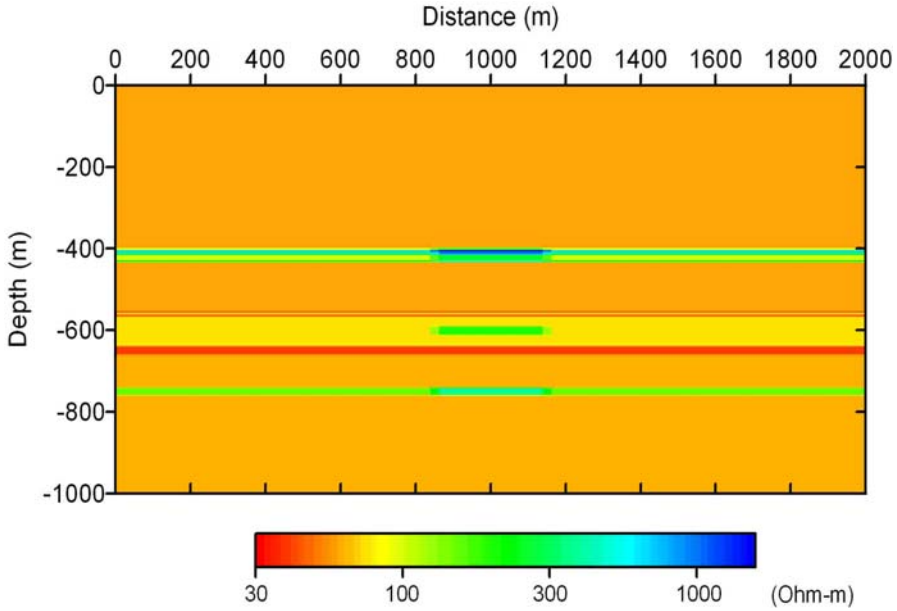

Figure 27b. 2D resistivity model for CO_2 injection in all three injection zones

Figure 28a compares the ratios of Mod1/Mod0 EM responses calculated using the 2D numerical method (Newman and Alumbaugh, 1997) (black curves) and using 1D method (red curves). Similarly, Figure 28b compares the ratios of Mod2/Mod0 EM responses calculated using the 2D numerical method (black curves) and using 1D method (red curves). The values obtained from the 1D method are significantly larger than those obtained by the 2D method. This is understandable because in the 1D model the whole layer (infinite extent) is CO_2 saturated while in the 2D model the CO_2 zone is only 300 m wide. The 2D EM responses clearly identify lateral boundaries of the injection zones, which are located between 850 m and 1150 m. If we focus on the EM data within the injection zones, we found that the slopes in the 1D and 2D data show some similarities even though the slopes from 2D calculation are sharper than those

obtained from the 1D method. They increase with the increasing source-receiver offsets, and the gradients are functions of the target resistivity. As a result, we may incorporate that information into our inversion.

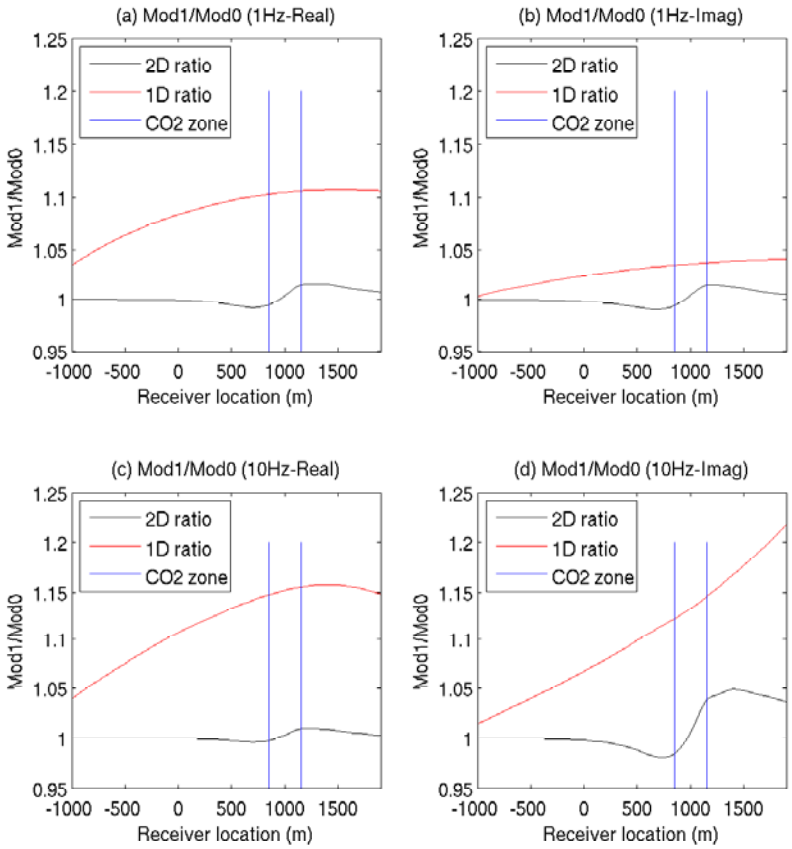

Figure 28a. Comparison between the real and imaginary components of EM data (ratio of Mod1/Mod0) calculated using the 2D numerical model (black curves) and those calculated using the 1D model (red curves). The response for frequency of 1 Hz is shown in (a) and (b), and the response for frequency of 10 Hz in shown in (c) and (d). The regions within the blue vertical parallel lines are CO_2 injection zones.

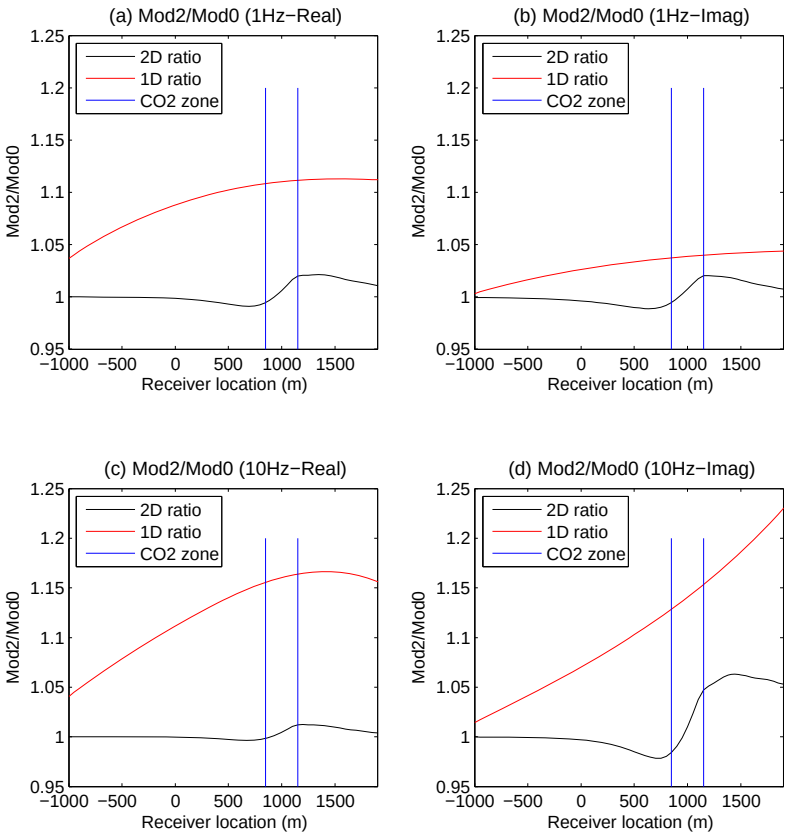

Figure 28b. Comparison between the real and imaginary components of EM data (ratio of Mod2/Mod0) calculated using the 2D numerical model (black curves) and those calculated using the 1D model (red curves). The response for frequency of 1 Hz is shown in (a) and (b), and the response for frequency of 10 Hz in shown in (c) and (d). The regions within the blue vertical parallel lines are CO_2 injection zones.

AVA Analysis

Our current AVA analysis is using the Bayesian model with 1D seismic and EM codes. This model is a revision of the joint inversion model given by Chen et al. (2007). The detail description of this model is given in Appendix 1. Since we use the 1D approximation of 2D seismic and EM data, the first step in our analysis was to compare 1D and 2D data (see above). Our 1D seismic convolution model provides good approximation to the 2D seismic data at small incident angles. The 1D EM model provides a fair approximation to the 2D EM data at the receivers right above the injection zones.

We jointly inverted time-lapse seismic and EM data for CO_2 saturation, and compared these inversion results with those obtained from the inversion of seismic data only. The results for the model with CO_2 injection in the top injection zone are given in Table 3 and Figure 29. Figure 29a shows the estimated probability density functions (pdfs) of the unknown CO_2 saturation using seismic AVA data only, while Figure 29b shows the estimated pdfs using both seismic AVA and EM data. In both cases, the inversion correctly predicts the presence of high CO_2 saturation in the injection zone. Incorporation of EM data significantly reduces inversion uncertainty since the pdfs obtained using both seismic and EM data are much sharper than those obtained using seismic data only. Table 3 also shows that standard error and

95% probability intervals of the unknown CO_2 saturation are lower if EM data are used in addition to seismic data.

Table 3. Comparison between the CO_2 saturation estimated using seismic AVA data only and that estimated using both seismic AVA and EM data for the case of one injection zone.

	Median	Mean	Mode	Standard deviation	95% Predictive Interval
CO_2 saturation (seismic AVA data only)	0.9844	0.9791	0.9891	0.0183	(0.9341, 0.9994)
CO_2 saturation (both seismic AVA and EM data)	0.9999	0.9999	0.9999	0.0001	(0.9995, 1.0000)

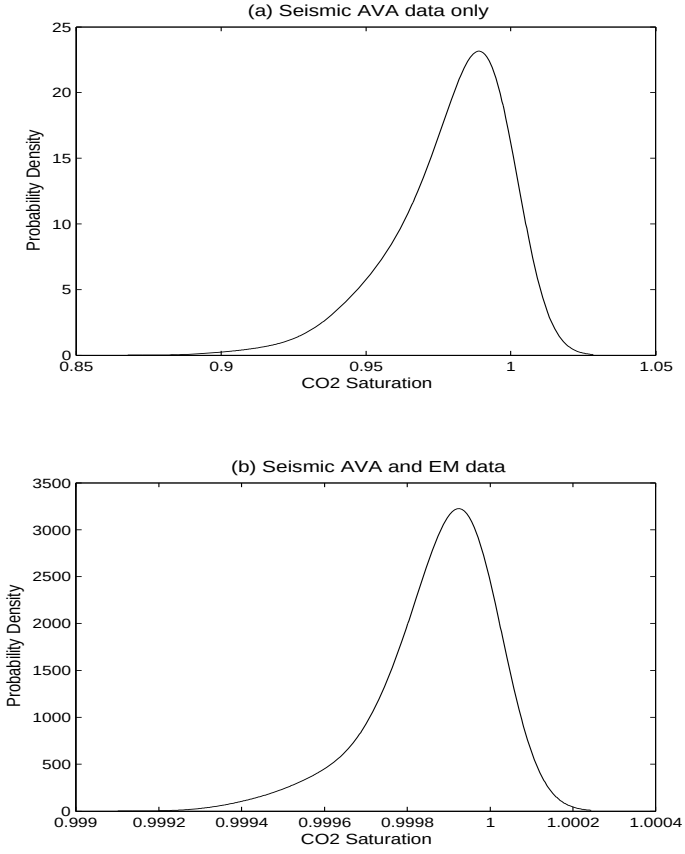

Figure 29. Estimated probability density functions (pdfs) of CO_2 saturation in the top injection zone (a) using seismic AVA data only, and (b) using both seismic AVA and EM data

The results for the model with CO_2 injection in three injection zones are given in Table 4 and Figure 30. Figures 30a-c show the estimated probability density functions (pdfs) of the unknown CO_2 saturation using seismic AVA data only, while Figures 30d-f show the estimated pdfs using both seismic AVA and EM data. Again, for the top two injection zones, the estimated CO_2 saturations are close to 1.0 with a

small uncertainty, and the joint inversion of seismic AVA and EM data improves the estimation by reducing uncertainty significantly (Figures 30a-b, 30d-e). The advantage of EM data is clearly illustrated in Figure 30c and Figure 30f. The inversion of seismic AVA data gives misleading results and shows the injection zone with a low CO_2 saturation (Figure 30c). This is far away from the true value of 95% CO_2 saturation. However, the inversion results after incorporating EM data clearly show there is a high CO_2 saturation zone (Figure 30f).

Table 4. Comparison between the CO_2 saturation estimated using seismic AVA data only and that estimated using both seismic AVA and EM data for the case of three injection zones.

	Zones	Median	Mean	Mode	Standard deviation	95% Predictive Interval
Seismic AVA data only	Zone-1	0.9900	0.9855	0.9931	0.0140	(0.9495, 0.9997)
	Zone-2	0.9419	0.9303	0.9646	0.0528	(0.8217, 0.9976)
	Zone-3	0.1067	0.1152	0.0813	0.0781	(0.0046, 0.2611)
Seismic AVA and EM data	Zone-1	0.9996	0.9995	0.9997	0.0005	(0.9979, 1.0000)
	Zone-2	0.9984	0.9978	0.9987	0.0020	(0.9928, 0.9999)
	Zone-3	0.9993	0.9991	0.9994	0.0008	(0.9972, 1.0000)

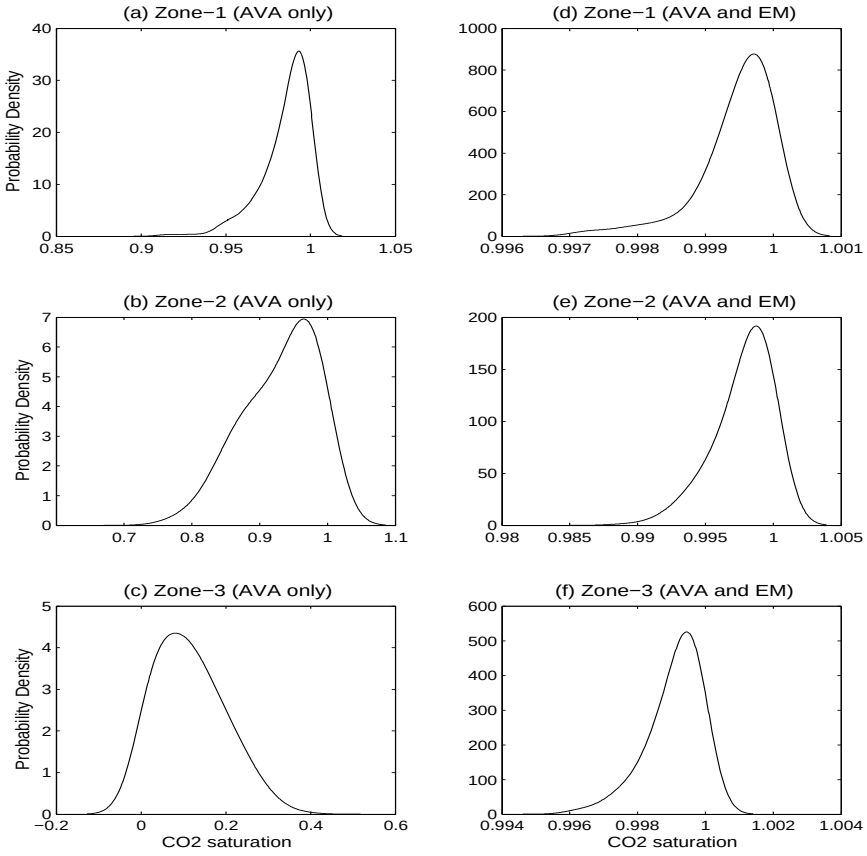

Figure 30. Estimated probability density functions (pdfs) of CO_2 saturation in three injection zones (a-c) using seismic AVA data only, and (d-f) using both seismic AVA and EM data.

In all cases, the joint inversion of seismic AVA and EM data gives higher CO_2 saturation than the corresponding true value (95%). This is possibly because the 1D approximation of 2D EM data underestimates the slopes in the EM data sets. To obtain more accurate results, and account for effects of finite site target zones, we may need to use 2D forward code in our inversion approach.

Even though there is an uncertainty in a rock-physics model and a discrepancy between 1D and 2D models, we found that by inverting seismic and EM data jointly, we can obtain much better estimates of CO_2 saturation, especially in the third injection zone where seismic AVA data fail to detect the high CO_2 saturation. Our synthetic studies show that time-lapse surface seismic and EM methods are a promising tool for CO_2 injection monitoring in the scenario presented in this study, however further studies are needed for more complicated scenarios.

8. Conclusions

- Literature reviews and contacts with other researchers have been conducted to obtain data on the geophysical properties of coal undergoing CO_2 flood. No quantitative relationships (tabulated values) of acoustic velocity, shear velocity, density or electrical resistivity as a function of CO_2 saturation have been found.
- A relationship between seismic velocity, water saturation and CO_2 saturation in a coal has been developed based on laboratory experiments conducted at LBNL. Seismic velocities were reduced on the order of 10% by the CO_2 flood.
- A relationship between electrical resistivity, water saturation and CO_2 saturation in coal has been developed based on laboratory experiments at LBNL. Electrical resistivity increased by 160% in the core when flooded by CO_2.
- The coal density as a function of CO_2 saturation under pressure and temperature conditions used in the flow simulation model was calculated using NIST14 code. The presence of CO_2 reduces the bulk density of the coal layer, causing the decrease in the gravity response. Adsorption of CO_2 into coal can affect the matrix density, and hence the total density change could be smaller than we predicted. The spatial pattern of the change in the vertical component of gravity is directly correlated with the net change in density of the coalbed.
- Sonic, density and resistivity well-logs, from a deep disposal well a couple of miles from the pilot test site, were used to construct background geophysical models used in sensitivity studies.
- The sensitivity studies showed that while the response to the 300 tons of CO_2 injected into a single layer wouldn't produce measurable surface response for either gravity or EM, the response due to an industrial-size injection would produce measurable surface signal for both techniques.
- Inversion of gravity data is very important, since construction of density contrast models significantly increases the amount of information that can be extracted from the gravity data. We developed a new approach that uses a depth of the reservoir as *a priori* information and solves for a smooth density variation inside the reservoir. The inversion results illustrated that, provided we can collect high-quality gravity data in the field and we have some a priori information about the depth of the reservoir, we can recover the spatial location of CO_2 plume correctly, although with the smoothing constraint of the inversion, the area was slightly overestimated, resulting in an underestimated value of density change.
- Even though there was an uncertainty in a rock-physics model and a discrepancy between 1D and 2D models, AVA analysis showed that by inverting seismic and EM data jointly, we can reduce uncertainty and obtain much better estimates of CO_2 saturation, especially in the third injection zone, where seismic AVA data fail to detect the high CO_2 saturation.
- Analysis of spatial resolution and detectability limits show that gravity and EM measurements could, under certain circumstances, be used as a lower-cost alternative to seismic measurements.

9. References

Aki, K., and Richards, P.G., 1980, Quantitative Seismology: Theory and methods: W.H. Freeman and Co.

Brown, J. M., T. Chen, T. M. Niebauer, F. J. Klopping, J. Ferguson, and J. Brady, 2003, Absolute and relative gravity integration for high precision 4D reservoir monitoring: EAGE Expanded Abstracts, A26-A26.

Chen, J., M. Hoversten, D. Vasco, Y. Rubin and Z. Hou, 2007, A Bayesian model for gas saturation estimation using marine seismic AVA and CSEM data, Geophysics, **72**, WA85-WA95.

Gasperikova, E., and M. Hoversten, 2006, A Feasibility Study of Non-seismic Geophysical Methods for Monitoring Geologic CO_2 Sequestration: The Leading Edge, **25,** 1282-1288.

Hare, J.L., J.F. Ferguson, and C.L.V. Aiken, 1999, The 4-D Microgravity Method for Waterflood Surveillance: A Model Study from the Prudhoe Bay Reservoir, Alaska: Geophysics, **64**, 78-87.

Kneafsey, T, Gritto, R., and Tomutsa, L., 2005, Coalbed methane laboratory experiments, LBNL report.

Levander, A.R., 1988, Fourth-order finite-difference P-SV seismograms: Geophysics, 53, 1425-1436.

Newman, G., and D. L. Alumbaugh, 1997, Three–dimensional massively parallel electromagnetic inversion—I. Theory: Geophysical Journal International, **128**, 345–354.

NIST Mixture Property Database, NIST Standard Reference Database #14, 1992, U.S. Department of Commence, National Institute of Standards and Technology (NIST).

Nooner, S.L., M.A. Zumberge, O. Eiken, T. Stenvold, and G.S. Sasagawa, 2003, Seafloor Micro-gravity Survey of the Sleipner CO_2 Sequestration Site: EOS Trans. AGU, **84**(46), Fall Meet. Suppl., Abstract GC31A-01.

Pashin, J.C., and P.E. Clark, 2006, SECARB Field Test for CO_2 Sequestration in Coalbed Methane Reservoirs of the Black Warrior Basin: Tuscaloosa, Alabama, University of Alabama, College of Continuing Studies, 2006 International Coalbed Methane Symposium Proceedings, paper 0630.

Smith, J.T., G.M. Hoversten, E. Gasperikova, and H.F. Morrison, 1999. Sharp Boundary Inversion of 2-D Magnetotelluric Data: Geophysical Prospecting, **47**, 469-486

10. Publications

Cohen, K., and Plasynski, S., 2008, Advancing Coal-Based Power Generation With Carbon Capture and Storage (CCS): Update of U.S. Department of Energy's (DOE) Global CCS Demonstration Role on Four Continents, Seventh Annual Conference on Carbon Capture and Sequestration, Pittsburgh, PA.

Gasperikova, E., and Hoversten, M., 2008, Gravity monitoring of CO_2 movement during sequestration: Model Studies: Geophysics, 73, No. 6, in press.

Gasperikova, E., 2008, A resolution study of non-seismic geophysical monitoring tools for CO_2 Enhanced CBM Production, Seventh Annual Conference on Carbon Capture and Sequestration, Pittsburgh, PA.

Kieke, D., and Imbus, S., 2008, The CO_2 Capture Project Phase 2 (CCP2) Storage Program: Progress in Geological Assurance, Seventh Annual Conference on Carbon Capture and Sequestration, Pittsburgh, PA.

Kieke, D. et al., 2008, The CO_2 Capture Project Phase 2 (CCP2) Storage Program: Progress in Geological Assurance in Unmineable Coal Beds, GHGT9, Washington D.C.

11. List of Acronyms and Abbreviations

CBM	Coal Bed Methane
CO_2	Carbon dioxide
Ex	Electric field in x-direction
Ey	Electric field in y-direction
EM	Electromagnetic
EOR	Enhanced Oil Recovery
Im	Imaginary part of a complex number
μGal	Microgal (gravity unit)
NIST	National Institute of Standards and Technology
Re	Real part of a complex number
Rx	Receiver
S	Saturation, (S_{CO2} = CO_2 saturation, S_g = gas saturation)
Tx	Transmitter

12. Acknowledgments

This work was supported in part by a Cooperative Research and Development Agreement between BP Corporation North America, as a part of the CO_2 Capture Project of the Joint Industry Program, and the U.S. Department of Energy, and by the Lawrence Berkeley National Laboratory under contract DE-AC02-05CH11231.

13. Report Appendices

APPENDIX 1

Monitoring of CO_2 injection into a coal bed using time-lapse seismic and EM data

Jinsong Chen, Erika Gasperikova, and Valeri Korneev

Lawrence Berkeley National Laboratory

One Cyclotron Road, MS: 90R1116

Berkeley, CA 94720

ABSTRACT

In this study, we investigate the feasibility of monitoring of CO_2 injection into a coalbed methane formation using time-lapse seismic and electromagnetic (EM) methods. At this injection site, there are three potential injection zones at depths from 400 m to 750 m and with a lateral extent of 300 m. Since inversion of 2D (or 3D) seismic and EM data is computational intensive and hence time-consuming, we use an 1D convolution model to approximate 2D seismic data, and an 1D layered model to approximate 2D EM data. Comparison between the 1D and 2D seismic and EM data shows that (1) the 1D convolution model provides a good approximation to the 2D seismic data at small incident angles, and (2) the 1D layered EM model provides a fair approximation to the 2D EM data at the receivers right above the injection zones. We jointly invert time-lapse seismic and EM data for CO_2 saturation, and compare these inversion results with those obtained from the inversion of seismic data only. Even though there is an uncertainty in a rock-physics model and a discrepancy between 1D and 2D models, we found that by inverting seismic and EM data jointly, we can obtain much better estimates of CO_2 saturation, especially in the third injection zone where seismic AVA (amplitude vs. angle) data fail to detect the high CO_2 saturation. Our synthetic studies show that time-lapse surface seismic and EM methods are a promising tool for CO_2 injection monitoring in the scenario presented in this paper, however further studies are needed for more complicated scenarios.

INTRODUCTION

It has been recognized that monitoring a field-scale CO_2 saturation is important for CO_2 sequestration. Time-lapse geophysical methods, for example, surface seismic and electromagnetic (EM), have the potential of providing this information, and hence being candidate monitoring tools. However, analyzing and inverting two- (2D) or three-dimensional (3D) geophysical data is still challenging and time-consuming. In this study, we explore the use of a joint inversion of seismic AVA (amplitude vs. angle) and EM data for estimating of CO_2 saturation. We will first compare the calculated seismic AVA and EM responses using the 2D numerical methods with those using one-dimensional (1D) methods, and then invert the 2D data using 1D approximation.

APPROXIMATION OF 2D GEOPHYSICAL DATA

In this section, we compare synthetic 2D seismic and EM data with those obtained from their corresponding 1D models for common seismic and EM profiles. The comparison will justify the use of 1D models as approximations to the 2D numerical models. The comparison will also provide insight into how to use the 1D models.

Seismic data

We compare seismic data based on the seismic attribute profile obtained from velocity and density logs from nearby well. There are three potential injection zones. We calculate seismic responses using 2D finite-difference staggered-grid code which models elastic wave propagation in arbitrarily inhomogeneous media (Levander, 1988), and 1D

convolution methods (Chen et. al., 2007) for the following three cases: (1) background (pre-injection) model (Model-0) using the well logs from nearby well, (2) model with a 10% decrease in P-wave velocity and a 5% decrease in density in the first injection zone (Model-1), and (3) model with the 10% decrease in P-wave velocity and the 5% decrease in density in all the three injection zones (Model-2). The decrease in P-wave velocity and density due to the presence of CO_2 was based on our laboratory measurements on coal samples (Kneafsey et al., 2005).

The 1D seismic data are calculated by convolving seismic reflectivity with a given wavelet. In this case, we use the Gaussian derivative wavelet with the center frequency of 18 Hz. Seismic AVA reflectivity is a explicit function of seismic P- and S-wave velocities and density in the given layers. We use the Zoeppritz equations (Aki and Richards, 1980) to model the reflectivity, which is a function of seismic P- and S-wave velocities and density in the background model (Model-0). Those values in Model-1 and Model-2 are the summation of the values in the background model and the changes due to the presence of CO_2.

Figures 1 and 2 compare the normalized differences (i.e., (Model-1 minus Model-0)/Model-0, and (Model-2 minus Model-0)/Model-0) in seismic AVA data caused by injection of CO_2 using the 2D (black curves) and 1D (red curves) models. Overall, the differences obtained from the 1D convolution model are close to those obtained from the 2D codes. In Figures 3 and 4, we take the first-order spatial difference of the seismic data shown in Figures 1 and 2. The discrepancies between the data calculated from 1D and 2D models are smaller than those without taking the first-order spatial difference. Although

the inversion results using the two types of data sets are very similar, we prefer to use the data after taking the first-order difference because it gives smaller data misfits.

EM data

2D EM model is based on a resistivity log from a nearby well. Model geometry is the same as in the seismic model; Model-0 is the background model, Model-1 is the model with CO_2 present in the top injection zone, and Model-2 is the model with CO_2 present in all three injection zones. The CO_2 injection zones are between x = 850 m and 1150 m. Again, the change in resistivity due to the CO_2 presence was based on our laboratory measurements (Kneafsey et al., 2005). We use both the 1D and 2D numerical methods to calculate EM responses for a given frequency, and source and receiver locations. We consider two frequencies (1 Hz and 10 Hz), five sources (x = -2000 m, -1900 m, -1800 m, -1700 m, and -1600 m, respectively), and sixty receivers from -1000 m to 1900 m with an interval of 50 m.

Figure 5 compares the ratios of Model-1/Model-0 EM responses calculated using the 2D numerical method (Newman and Alumbaugh, 1997) (black curves) and using 1D method (red curves). Similarly, Figure 6 compares the ratios of Model-2/Model-0 EM responses calculated using the 2D numerical method (black curves) and using 1D method (red curves). From both figures, we can see that the EM responses due to the presence of CO_2 injection zones are very different in terms of values. The values obtained from the 1D method are significantly larger than those obtained by the 2D method. This is understandable because in the 1D model the whole layer (infinite extent) is CO_2 saturated while in the 2D model the CO_2 zone is only 300 m wide. The 2D EM responses clearly

identify lateral boundaries of the injection zones, which are located between 850 m and 1150 m. If we focus on the EM data within the injection zones, we found that the slopes in the 1D and 2D data show some similarities even though the slopes from 2D calculation are sharper than those obtained from the 1D method. They increase with the increasing source-receiver offsets, and the gradients are functions of the target resistivity. As a result, we may incorporate that information into our inversion.

BAYESIAN MODEL

In this section, we briefly show the Bayesian model for a joint inversion of 1D seismic AVA and EM data. We first show likelihood functions for seismic AVA and EM data based on the 1D approximation to the 2D data, then we show the prior distribution, and finally we give the sampling methods for drawing samples from the joint posterior probability distribution functions. The developed Bayesian model is an revision of the joint inversion model given by Chen et. al. (2007).

Geophysical data

The geophysical data used for this study are time-lapse seismic AVA and EM data. Let vectors $\mathbf{v}_p^{(bg)}$, $\mathbf{v}_s^{(bg)}$, and $\boldsymbol{\rho}^{(bg)}$ represent the background model seismic P- and S-wave velocities and density for 40 layers. Let a vector $\mathbf{r}^{(bg)}$ be the electrical resistivity in the same background model. The seismic AVA and EM responses of the background model are given as follows:

$$\mathbf{Y}_{AVA}^{(bg)} = G_1(\mathbf{v}_p^{(bg)}, \mathbf{v}_s^{(bg)}, \boldsymbol{\rho}^{(bg)}), \tag{1}$$

and

$$\mathbf{Y}_{EM}^{(bg)} = G_2(\mathbf{r}^{(bg)}). \quad (2)$$

The presence of CO_2 in the injection zone causes a decrease in seismic velocity and density and an electrical resistivity increase. Let vectors $\Delta\mathbf{v}_p$, $\Delta\mathbf{v}_s$, $\Delta\boldsymbol{\rho}$, and $\Delta\mathbf{r}$ represent the changes caused by the CO_2 saturation in seismic P-wave and S-wave velocities, density and electrical resistivity, respectively . Notice that typically $\Delta\mathbf{v}_s$ is equal to zero as in this study. Thus, the time-lapse seismic data are the difference between the seismic AVA responses before and after the injection, which are given by:

$$\mathbf{Z}^{(AVA)} = G_1(\mathbf{v}_p^{(bg)} + \Delta\mathbf{v}_p, \mathbf{v}_s^{(bg)} + \Delta\mathbf{v}_s, \boldsymbol{\rho}^{(bg)} + \Delta\boldsymbol{\rho}) - \mathbf{Y}_{AVA}^{(bg)}. \quad (3)$$

As shown in Figures 6 and 7, the first-order difference of the normalized differences has smaller variations, and therefore the seismic data used in this study are the differences given by $\mathbf{d}^{(AVA)} = \delta(\mathbf{Z}^{(AVA)})$

For EM data, we first calculate the ratios of EM responses between the model with and without CO_2 present, which is given below:

$$\mathbf{Z}^{(EM)} = G_2(\mathbf{r}^{(bg)} + \Delta\mathbf{r}) / \mathbf{Y}_{EM}^{(bg)}. \quad (4)$$

As shown in Figures 8 and 9, we use the EM data from the receivers at locations from 850 m to 1150 m. Therefore the EM data used in this study are given by $\mathbf{d}^{(EM)} = \mathbf{Z}^{(EM)} - \mathbf{Z}_{850}^{(EM)}$.

Stochastic Model

We developed a stochastic model to estimate unknown CO_2 saturation given the seismic AVA and EM data described above. Let vector $\mathbf{S}_g$ be the CO_2 saturation in the injection zones. If there is only one injection zone, we have one unknown variable. If

there are three injection zones, we have three unknown variables. The Bayesian model for the inversion is given below:

$$f(\mathbf{S}_g \mid \mathbf{d}^{(AVA)}, \mathbf{d}^{(EM)}) \propto f(\mathbf{d}^{(AVA)}, \mathbf{d}^{(EM)} \mid \mathbf{S}_g) f(\mathbf{S}_g) \tag{5}$$

The first term on the right side of Equation (5) is referred to as the likelihood functions, which is the link between seismic AVA and EM data and unknown CO_2 saturation. The second term on the right side of the equation is referred to as the prior distribution, which summarizes the information that is not included in the current data.

Likelihood Models

We assume that errors in seismic AVA data are independent of the errors in EM data, and thus we can write the likelihood function as the product of two terms:

$$f(\mathbf{d}^{(AVA)}, \mathbf{d}^{(EM)} \mid \mathbf{S}_g) \propto f(\mathbf{d}^{(AVA)} \mid \mathbf{S}_g) f(\mathbf{d}^{(EM)} \mid \mathbf{S}_g). \tag{6}$$

For seismic data, we assume that the total number of data is m, which is equal the product of the total number of incident angles and the total number of data points for each incident angle. We assume that errors in the seismic data have the normal distribution with zero mean and the standard error determined by a given signal-to-noise (S/N) ratio (5 in this study). Let $d_i^{(obsAVA)}$ represent the i-th AVA data and $a_i^{(calc)}$ represent the i-th calculated AVA data. Thus, we have

$$f(\mathbf{d}^{(AVA)} \mid \mathbf{S}_g) = \prod_{i=1}^{m} \frac{1}{\sqrt{2\pi}\sigma} \exp\left(-\frac{(d_i^{(obsAVA)} - a_i^{(calc)})^2}{2\sigma^2} \right). \tag{7}$$

Similarly, we can derive the likelihood function of EM data. Let n be the total number of EM data and σ_r be the relative errors in EM data (5% in this study). Let

$d_i^{(obsEM)}$ be the i-th EM data and $e_i^{(calc)}$ be the corresponding calculated EM responses. Thus, we obtain the following function:

$$f(\mathbf{d}^{(EM)} \mid S_g) = \prod_{i=1}^{n} \frac{1}{\sqrt{2\pi}\sigma_r} \exp\left(-\frac{1}{2\sigma_r^2} \left(\frac{d_i^{(obsEM)} - e_i^{(calc)}}{d_i^{(obsEM)}} \right)^2 \right). \tag{8}$$

Prior Model

The prior distribution is determined using prior knowledge and other information about the unknown parameters. We assume unknown CO_2 saturation in each zone are independent of each other. As a result, we can write the prior distribution as the product of several terms, given below:

$$f(\mathbf{S}_g) = f(S_{g1}) f(S_{g2}) f(S_{g3}) \tag{9}$$

We assume that CO_2 saturation in each zone is uniformly distributed on (0, 1).

MCMC Sampling Methods

We use Markov Chain Monte Carlo (MCMC) sampling methods to obtain estimates of unknown parameters from the Bayesian model defined in Equation (5). Unlike optimization-based methods seeking a single optimal solution of unknown parameters, MCMC sampling-based methods draw many samples from the joint posterior distribution. Using those samples, we can make inferences about the marginal distributions of each parameter, such as its mean, variance, and predictive intervals.

MCMC sampling methods have been found to be useful for inverting complex geophysical data set (e.g., Bosch, 1999; Malinverno, 2002; and Buland et al., 2003). The

main steps for using MCMC methods entail: (1) deriving conditional probability functions given all the data and other unknown variables, which are referred to as full conditional distribution functions; (2) generating samples using suitable algorithms; (3) making inferences about each unknown. In the following, we first show the full conditional distribution functions of unknown vectors given in Equation (1), and then describe the sampling algorithms used in this study, which include the Metropolis-Hasting methods (Hasting, 1970) and the slice sampling methods (Neil, 2003).

INVERSION RESULTS

In this section, we investigate the feasibility of using time-lapse seismic AVA and EM data to monitor CO_2 injection into coal beds through synthetic case studies. We assume that the background information, such as thickness of each layer, seismic P- and S-wave velocities, density, and electrical resistivity in each of these layers, can be obtained from borehole logging. The background models for seismic attributes and electrical properties may be different, but the CO_2 injection zones are located at roughly same depths in both models. Our main focus is on the following issues:

(1) Can seismic methods detect the change due to the CO_2 presence in the injection zones?

(2) How accurate are the seismic methods for quantitatively estimating those changes?

(3) What are the benefits of incorporating EM data into the estimation of CO_2 saturation?

We will try to answer above questions through two case studies.

Synthetic data

We consider three CO_2 injection zones in the seismic model in depths – (1) from 405 m to 442 m (thickness of 37 m), (2) from 592 m to 610 m (thickness of 8 m), and (3) from 740 m to 750 m (thickness of 10 m), respectively. The three injection zones in the resistivity model are slightly different; they are located at depth ranges of (1) 399 - 433 m (thickness of 34 m), (2) 590 - 611 m (thickness of 12 m), and (3) 740 - 760 m (thickness of 20 m). We consider two injection strategies. The first one (referred to as Model-1) injects CO_2 only into the first zone, and the second one injects CO_2 into all three zones (referred to as Model-2). The case of one injection zone is an ideal situation for monitoring CO_2 change using seismic and EM methods because we can avoid possible complex effects from multiple layers.

Synthetic seismic data were generated using a 2D finite-difference staggered-grid code which models elastic wave propagation in arbitrarily inhomogeneous media with a 18 Hz Gaussian derivative source wavelet (Levander, 1988). After normal moveout (NMO) correction, we created a common depth point (CDP) stack, and from that AVA data. We first generated seismic AVA for the background model, and then we assumed that the injection zone has 95% CO_2 saturation, and generated seismic AVA responses again. The differences in seismic AVA attributes are our time-lapse AVA data . As only first four incident angles (corresponding to 0, 1.9, 3.8, and 5.7 degrees, respectively) have responses to all the zones, we only use them for inversion. The comparison between 2D seismic data and 1D convolution approximation were given in Section 2.

Synthetic EM data were also generated using 2D numerical methods (Newman and Alumbaugh, 1997) at two frequencies (1 Hz and 10 Hz), with five transmitter locations (-2000 m, -1900 m, -1800 m, -1700 m, and -1600 m, respectively), and 60 receivers located from -1000 m to 1900 m with a separation of 50 m. Since only the changes in EM responses from the receivers between 850 m and 1150 m show similar patterns to those in 1D approximation (see Section 2), we assume that EM data are available only at seven receivers (850 m, 900 m, 950 m, 1000 m, 1050 m, and 1100 m, respectively). In summary, the EM data used in this inversion have two frequencies (1 Hz and 10 Hz), five transmitters, and seven receivers.

Rock physics model

It is difficult to obtain a reliable rock physic models for this study given limited information. Since our focus is on the change of CO_2 saturation in the injection zones, we only need relationships that tie the CO_2 changes to the changes of seismic attributes (e.g., seismic P- and S-wave velocities and density) and to the changes of electrical resistivity.

Our rock physics model is based on the following assumptions:

(1) Seismic S-wave velocity does not change with the change of CO_2 saturation.

(2) Seismic P-wave velocity and density linearly decrease with the increasing CO_2 saturation.

(3) Electrical resistivity linearly increases with the increasing CO_2 saturation.

(4) 95% CO_2 saturation leads to 10% decrease in seismic P-wave velocity, 5% decrease in density, and 150% increase in electrical resistivity.

Based on the above assumptions, we developed linear relationships between the changes in CO_2 saturation and the changes in seismic and electrical attributes. We assumed that the injection zone has 95% CO_2 saturation both in the seismic and EM model. Our rock physics model can be improved if more information is available.

One injection zone: Model-1

In the first case, we only inject CO_2 into the top injection zone (depths between 405 and 442 m). We strive to estimate CO_2 saturation from time-lapse seismic AVA and EM data sets. The prior distribution of the unknown CO_2 saturation is assumed to be uniform on (0, 1), and therefore it is non-informative.

Figure 7 shows the estimated probability density functions (pdfs) of the unknown CO_2 saturation. The curve in Figure 7a shows the estimated pdf using seismic AVA data only, and the curve in Figure 7b shows the estimated pdf using both seismic AVA and EM data. The results show that in both cases - using seismic data only and using both seismic and EM data the inversion correctly predicts the presence of high CO_2 saturation in the injection zone. Notice that the median, mean, and mode of the pdfs (see Table-1) are higher than the true value of 95%. The possible cause for the higher values are the discrepancies between 2D data and 1D approximations, and errors in the empirical rock physics model for linking the change in CO_2 saturation to the changes in seismic and electrical attributes.

In addition, by comparing the curve in Figure 7a with the one in Figure 7b, we found that the incorporation of EM data can significantly reduce uncertainty associated with the inversion since the pdf obtained using both seismic and EM data are much

shaper than that obtained using seismic AVA data only. Table-1 also shows that the standard error (5^{th} column), and 95% probability intervals (6^{th} column) of the unknown CO_2 saturation obtained using seismic AVA data only are larger than those obtained using both seismic and EM data.

Three injection zones: Model-2

In the second case, we assume that CO_2 is injected into three isolated injection zones. Therefore, we need to estimate three CO_2 saturations (one for each injection zone) from seismic AVA and EM data sets. We still use the non-informative prior for each unknown CO_2 saturation, with its uniform distribution on (0, 1).

As shown in Figure 8, for the first injection zone, we can see similar patterns to those seen in the first case study. The estimated CO_2 saturation is close to 1.0 with a small uncertainty, and the joint inversion of seismic AVA and EM data improves the estimation by reducing uncertainty significantly. For the second injection zone, the estimated CO_2 saturation is also close to 1.0, and uncertainty is little larger than that in the first injection zone. Again, the inclusion of EM data reduces uncertainty associated with the estimation.

For the third injection zone, the inversion of seismic AVA data gives misleading results and shows the injection zone with a low CO_2 saturation. This is far away from the true value of 95% CO_2 saturation. However, the inversion results after incorporating EM data clearly show there is a high CO_2 saturation zone.

In all the cases, the joint inversion of seismic AVA and EM data gives us higher CO_2 saturation than the corresponding true value (95%). This is possibly because the 1D

approximation of 2D EM data underestimate the slopes in the EM data sets. To obtain more accurate results, and account for effects of finite site target zones, we may need to use 2D forward code in our inversion approach.

DISCUSSION AND CONCLUSIONS

In this study we have demonstrated the utility of time-lapse seismic and EM for monitoring of CO_2 saturation in the coalbed methane environment using Bayesian stochastic inversion models. Through the synthetic studies, we have shown that

(1) 1D convolution methods can provide a good approximation for the 2D seismic data.

(2) The ratio of 2D EM responses for the model with and without CO_2 at the receivers located above the injection zones can be approximated using the ratio of 1D EM responses for the same models at the same receivers.

(3) Stochastic inversion of seismic AVA data can provide good estimates of CO_2 saturation in the first two injection zones.

(4) The incorporation of EM data can reduce uncertainty in the estimates of CO_2 saturation.

REFERENCES

Archie, G. E., 1942, The electrical resistivity log as an aid in determining some reservoir characteristics: Trans. Am. Inst. Mech. Eng., **146**, 54-62.

Bernardo, J. M. and Smith, A. F., 1994, Bayesian theory: John Wily and Sons, New York.

Bosch, M., 1999, Lithologic tomography: from plural geophysical data to lithology estimation: Journal of Geophysical Research, **104**, 749-766.

Buland, A., and Omre, H., 2003, Bayesian linearized AVO inversion: Geophysics, **68**, 185-198.

Chen, J., M. Hoversten, D. Vasco, Y. Rubin and Z. Hou, 2007, A Bayesian model for gas saturation estimation using marine seismic AVA and CSEM data, Geophysics, **72**, WA85-WA95.

Gilks, W., Richardson, S., and Spiegelhalter, D., 1996, Markov Chain Monte Carlo in Practice: Chapman & Hall/CRC, New York.

Kneafsey, T, Gritto, R., and Tomutsa, L., 2005, Coalbed methane laboratory experiments, LBNL report.

Levander, A.R., 1988, Fourth-order finite-difference P-SV seismograms: Geophysics, 53, 1425-1436.

Maliverno, A., 2002, Parsimonious Bayesian Markov chain Monte Carlo inversion in a nonlinear geophysical problem: Geophysical Journal International, **151**, 675-688.

Mosegaard, K. and Tarantola, A., 1995, Monte Carlo sampling of solutions to inverse problems: Journal of Geophysical Research, **100**, 12431-12447.

Newman, G., and D. L. Alumbaugh, 1997, Three–dimensional massively parallel electromagnetic inversion—I. Theory: Geophysical Journal International, **128**, 345–354.

TABLE 1. Comparison between the CO_2 saturation estimated using seismic AVA data only and that estimated using both seismic AVA and EM data for the case of one injection zone.

	Median	Mean	Mode	Standard deviation	95% Predictive Interval
CO_2 saturation (seismic AVA data only)	0.9844	0.9791	0.9891	0.0183	(0.9341, 0.9994)
CO_2 saturation (both seismic AVA and EM data)	0.9999	0.9999	0.9999	0.0001	(0.9995, 1.0000)

TABLE 2. Comparison between the CO_2 saturation estimated using seismic AVA data only and that estimated using both seismic AVA and EM data for the case of three injection zones.

	Zones	Median	Mean	Mode	Standard deviation	95% Predictive Interval
Seismic AVA data only	Zone-1	0.9900	0.9855	0.9931	0.0140	(0.9495, 0.9997)
	Zone-2	0.9419	0.9303	0.9646	0.0528	(0.8217, 0.9976)
	Zone-3	0.1067	0.1152	0.0813	0.0781	(0.0046, 0.2611)
Seismic AVA and EM data	Zone-1	0.9996	0.9995	0.9997	0.0005	(0.9979, 1.0000)
	Zone-2	0.9984	0.9978	0.9987	0.0020	(0.9928, 0.9999)
	Zone-3	0.9993	0.9991	0.9994	0.0008	(0.9972, 1.0000)

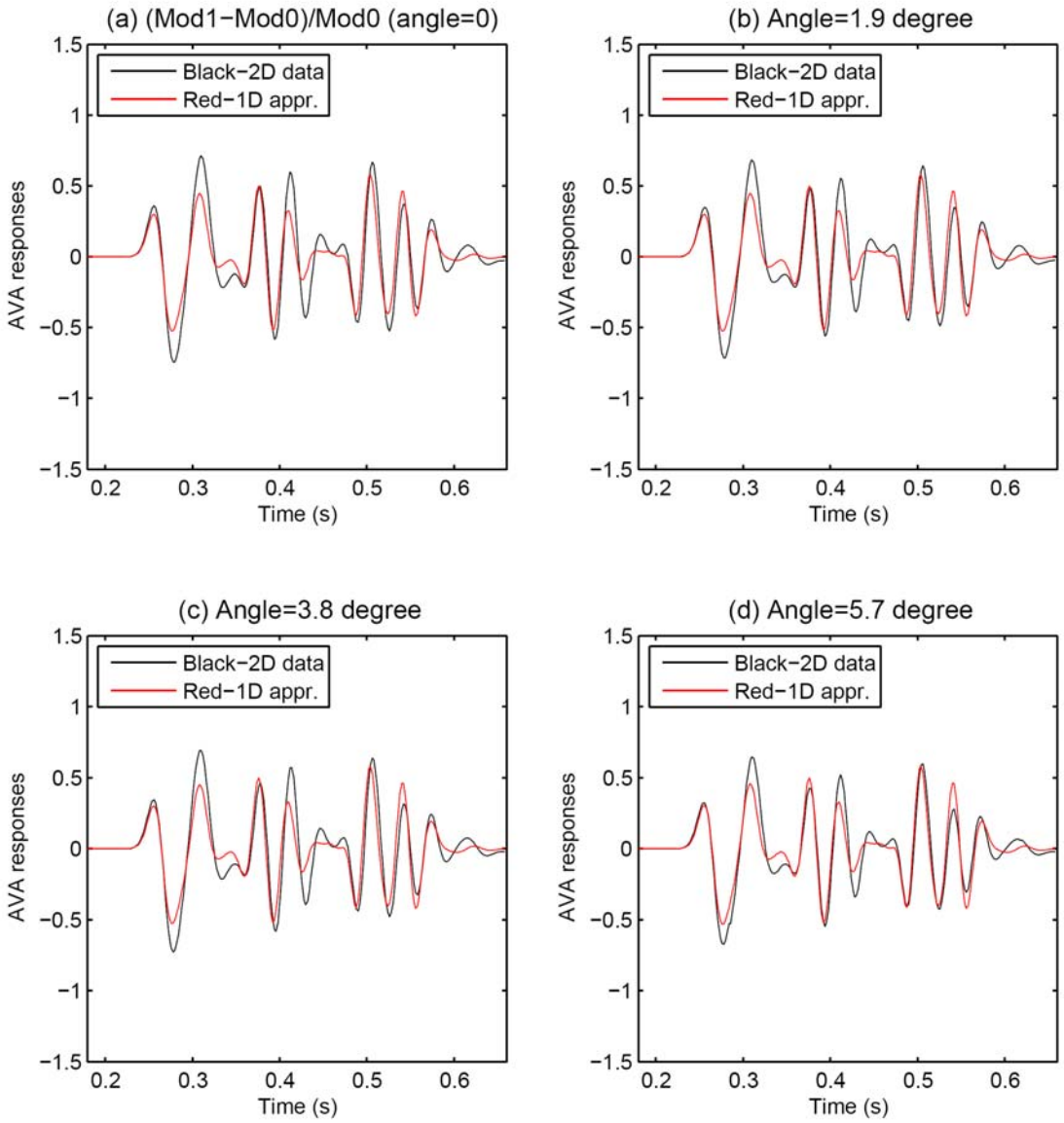

Figure 1: Comparison of differences in normalized seismic AVA data, (Model-1 - Model-0)/Model-0 for four angles, where the black curves are calculated using the 2D numerical methods and the red curves are calculated using the 1D convolution method.

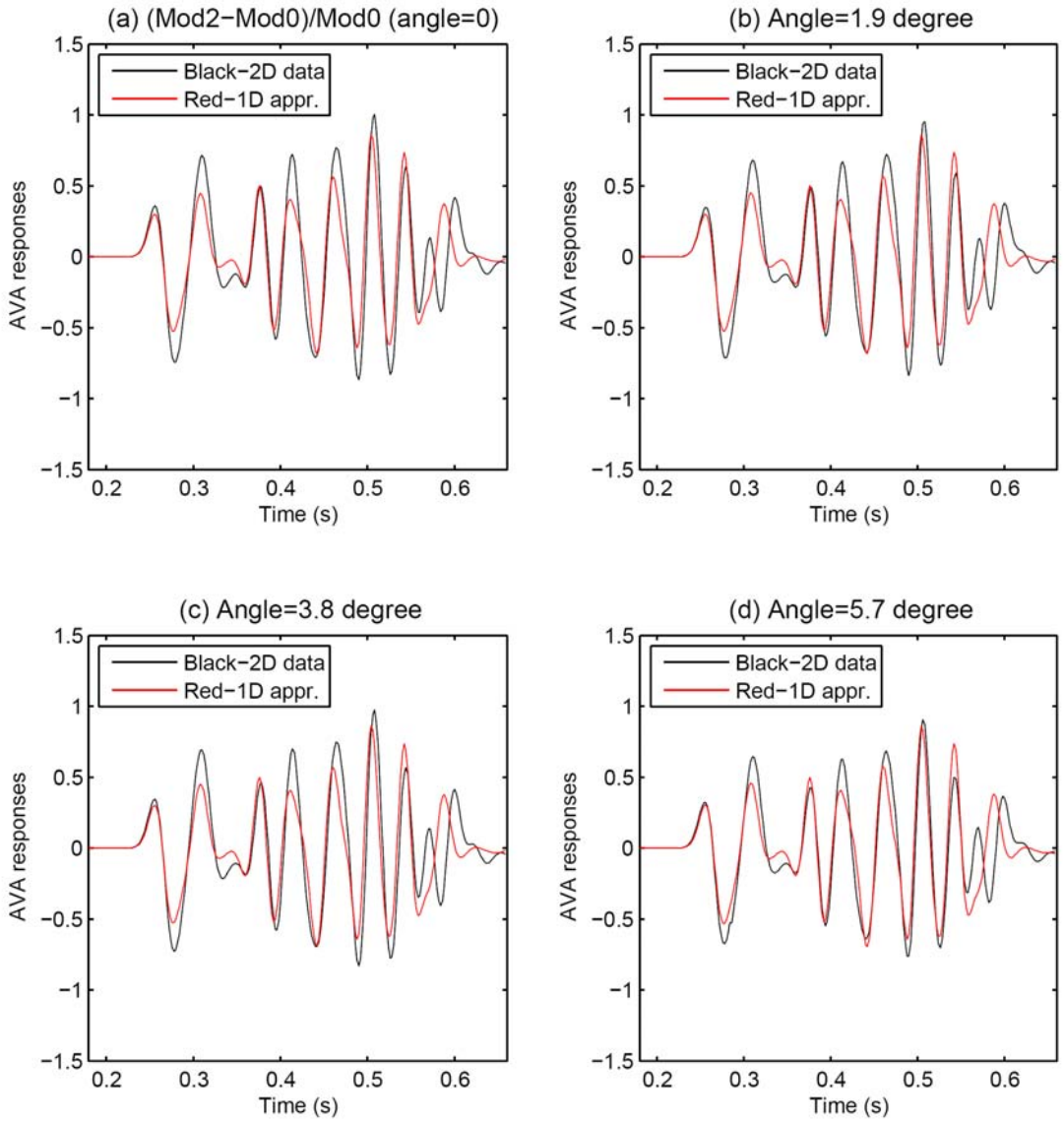

Figure 2: Comparison of differences in normalized seismic AVA data, (Model-2 – Model-0)/Model-0 for four angles, where the black curves are calculated using the 2D numerical methods and the red curves are calculated using the 1D convolution method.

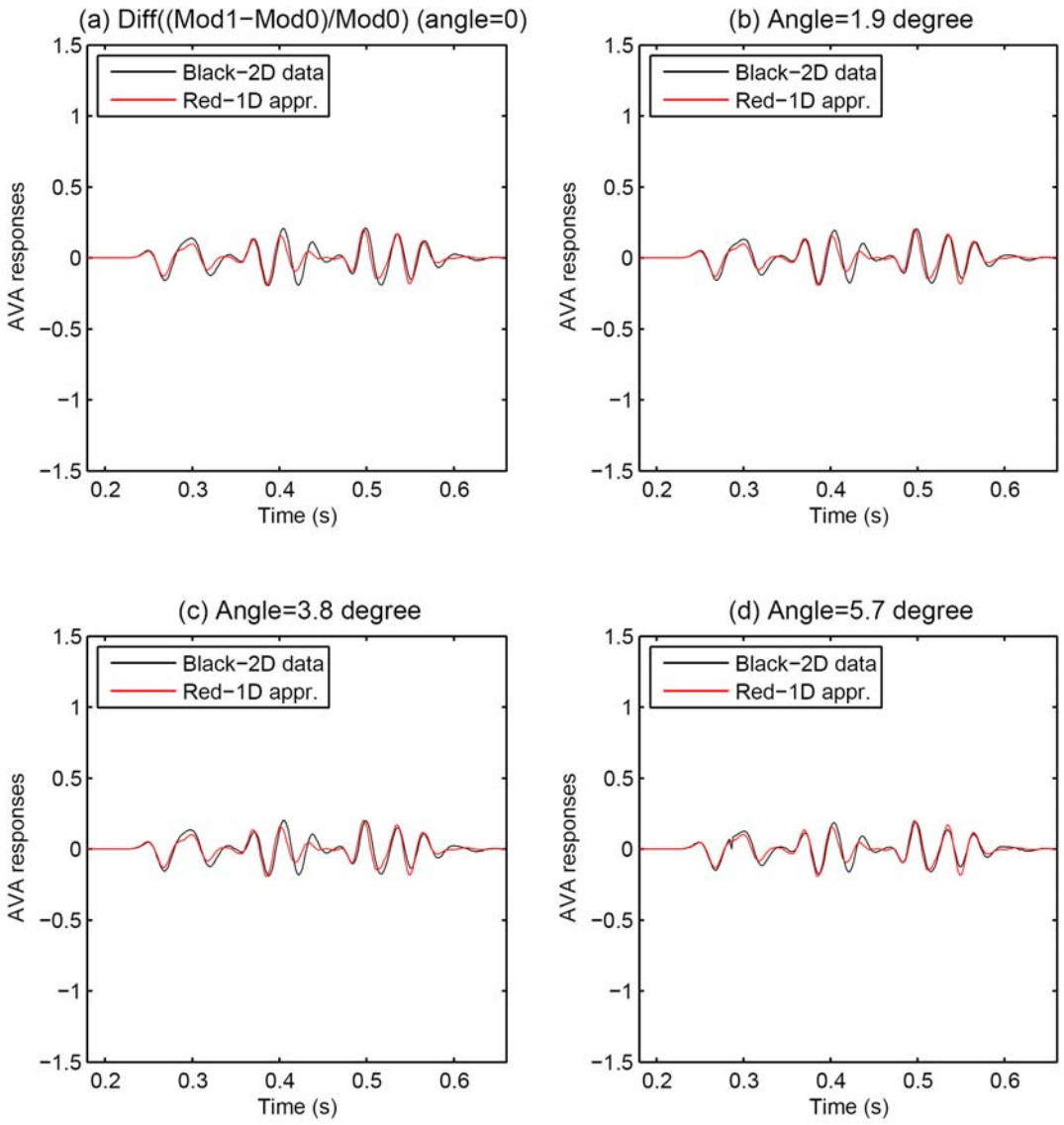

Figure 3: Comparison between the first-order spatial difference of seismic AVA data shown in Figure 1 using 2D codes (black curves) and 1D codes (red curves).

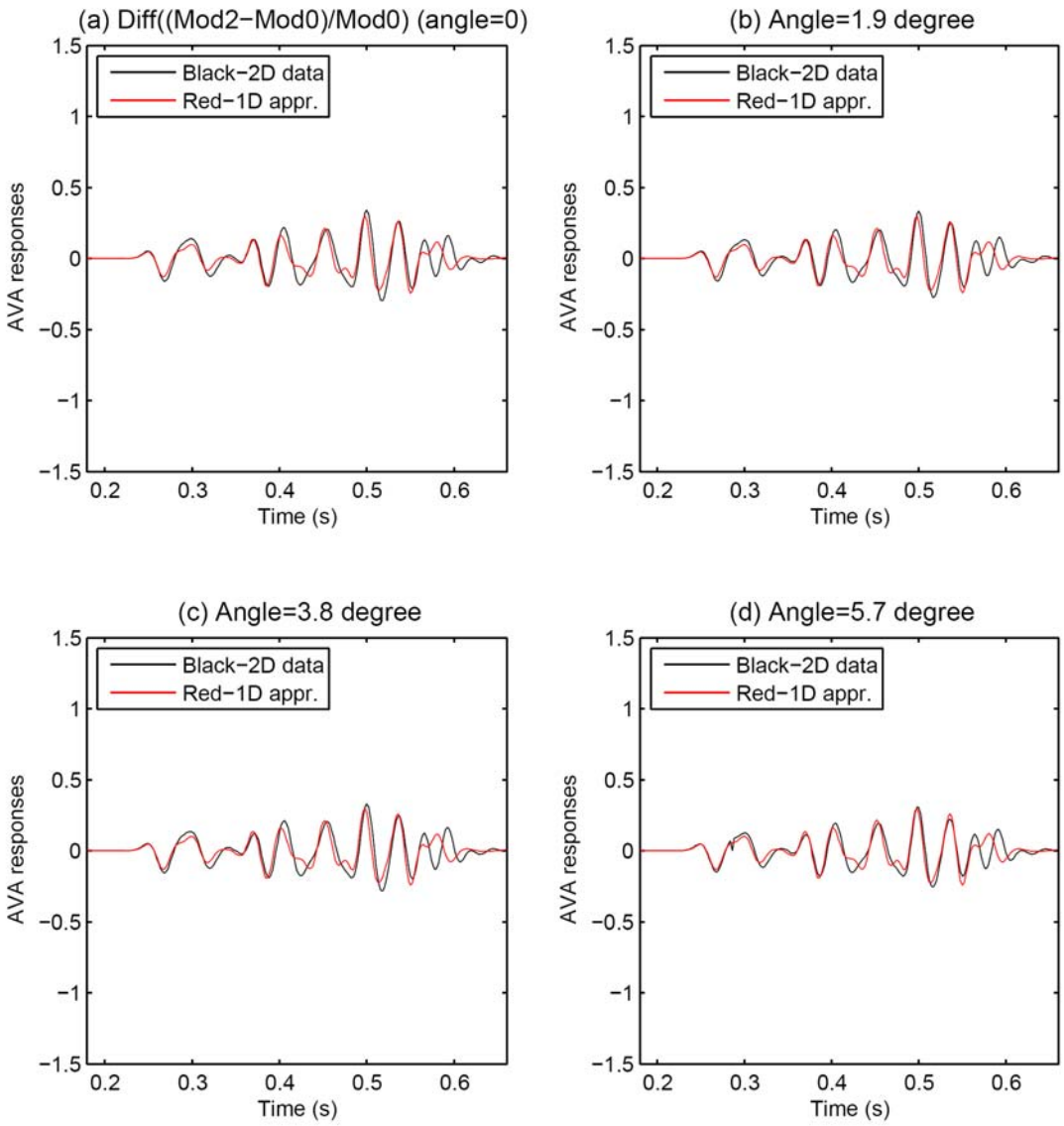

Figure 4: Comparison between the first-order spatial difference of seismic AVA data shown in Figure 2 using 2D codes (black curves) and 1D codes (red curves).

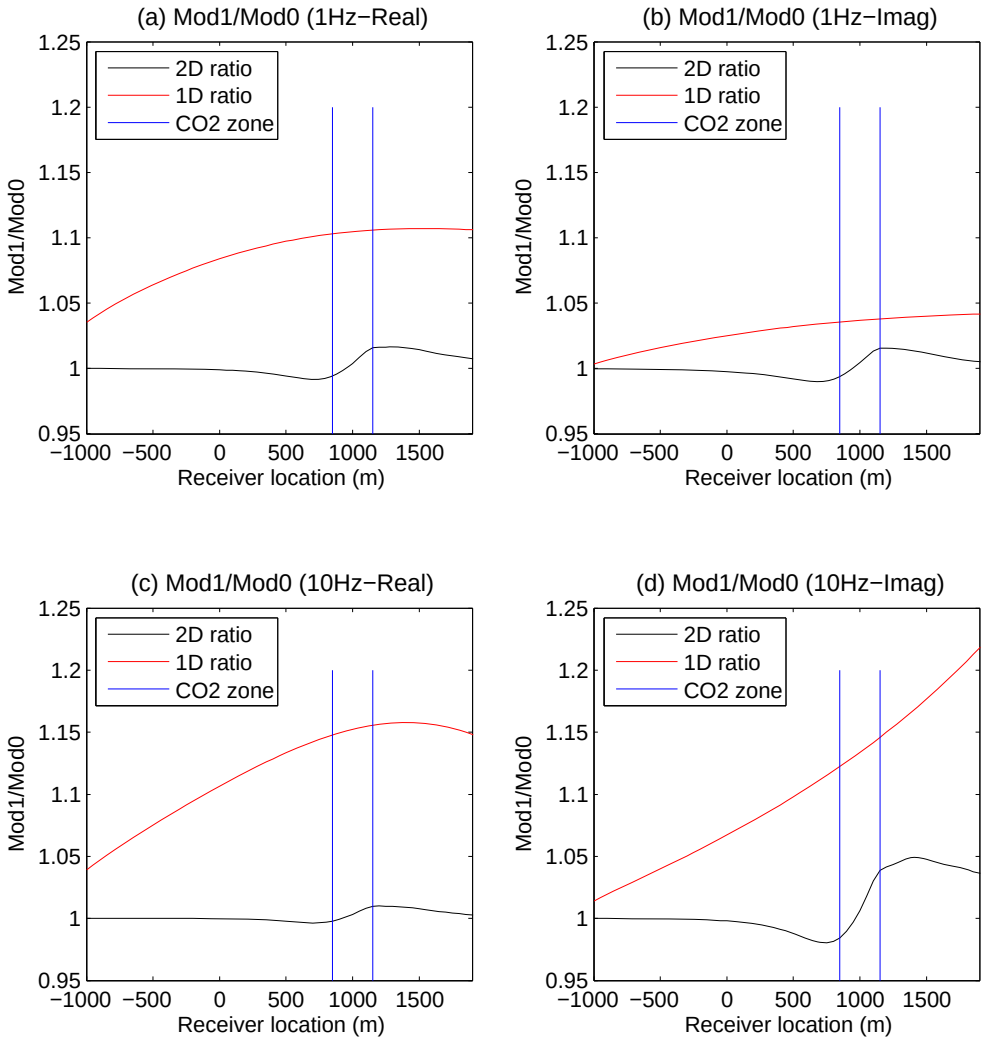

Figure 5: Comparison between the real and imaginary components of EM data (ratio of Model-1/Model-0) calculated using the 2D numerical model (black curves) and those calculated using the 1D model (red curves). The response for frequency of 1 Hz is shown in (a) and (b), and the response for frequency of 10 Hz in shown in (c) and (d). The regions within the blue vertical parallel lines are CO_2 injection zones.

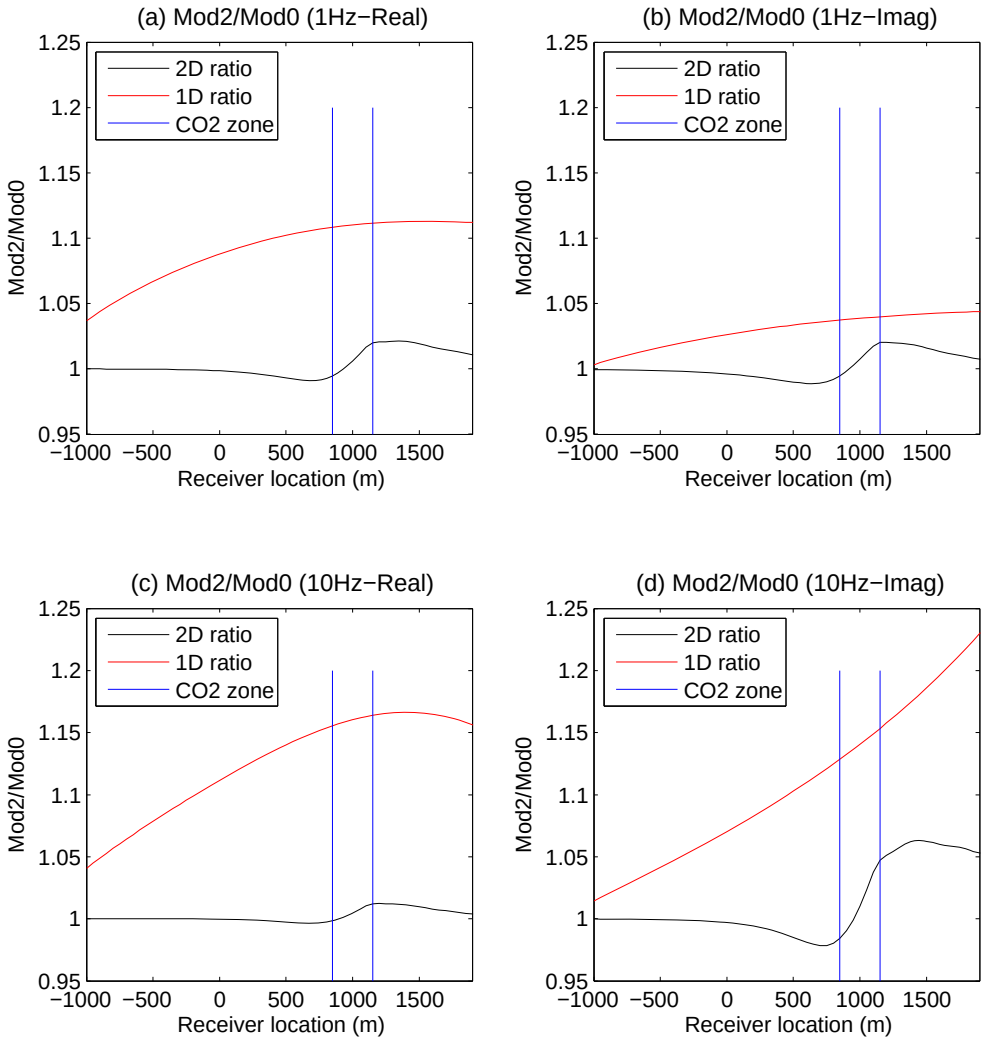

Figure 6: Comparison between the real and imaginary components of EM data (ratio of Model-2/Model-0) calculated using the 2D numerical model (black curves) and those calculated using the 1D model (red curves). The response for frequency of 1 Hz is shown in (a) and (b), and the response for frequency of 10 Hz in shown in (c) and (d). The regions within the blue vertical parallel lines are CO_2 injection zones.

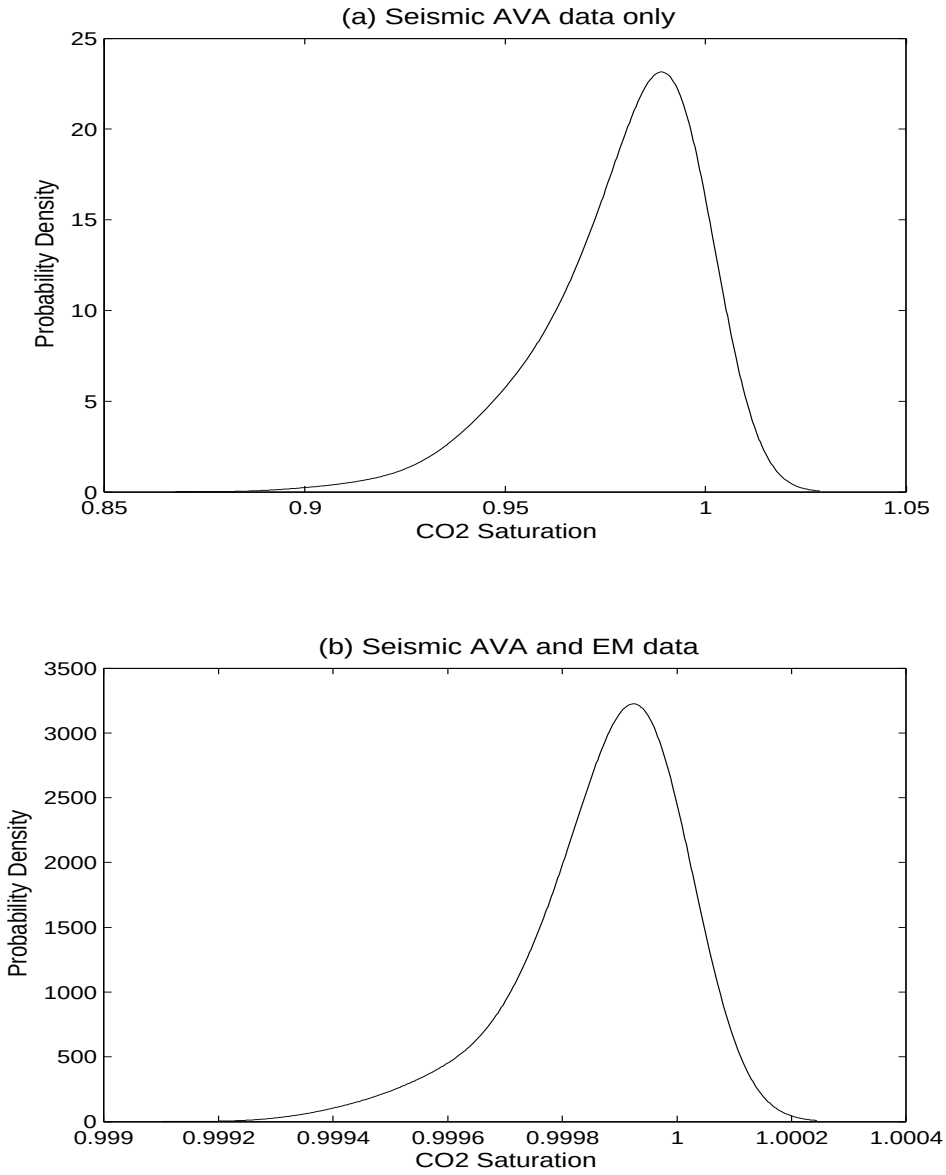

Figure 7: Estimated probability density functions (pdfs) of CO_2 saturation in the injection zone of Model-1: (a) using seismic AVA data only, and (b) using both seismic AVA and EM data.

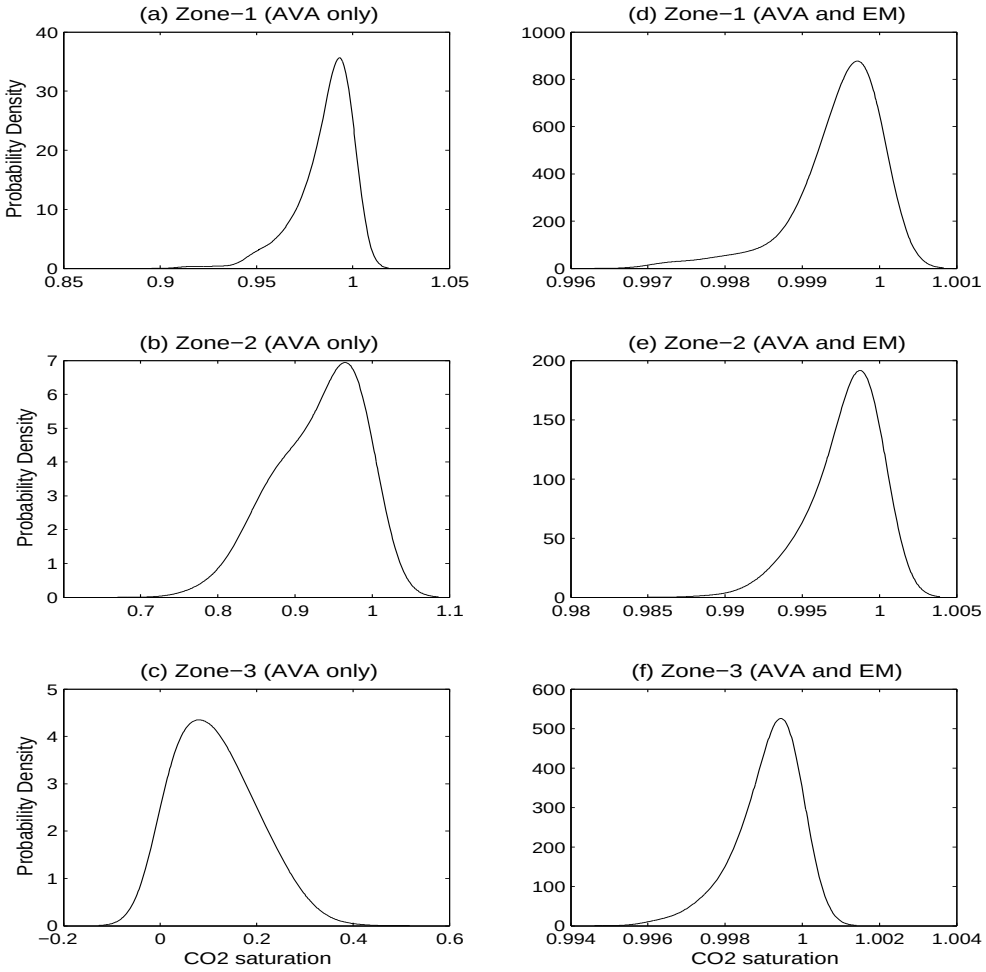

Figure 8: Estimated probability density functions (pdfs) of CO_2 saturation in the three injection zones of Model-2: (a-c) using seismic AVA data only, and (d-f) using both seismic AVA and EM data.